NGU
Norges geologiske undersøkelse
Geological Survey of Norway

GEOLOGI FOR SAMFUNNET
GEOLOGY FOR SOCIETY

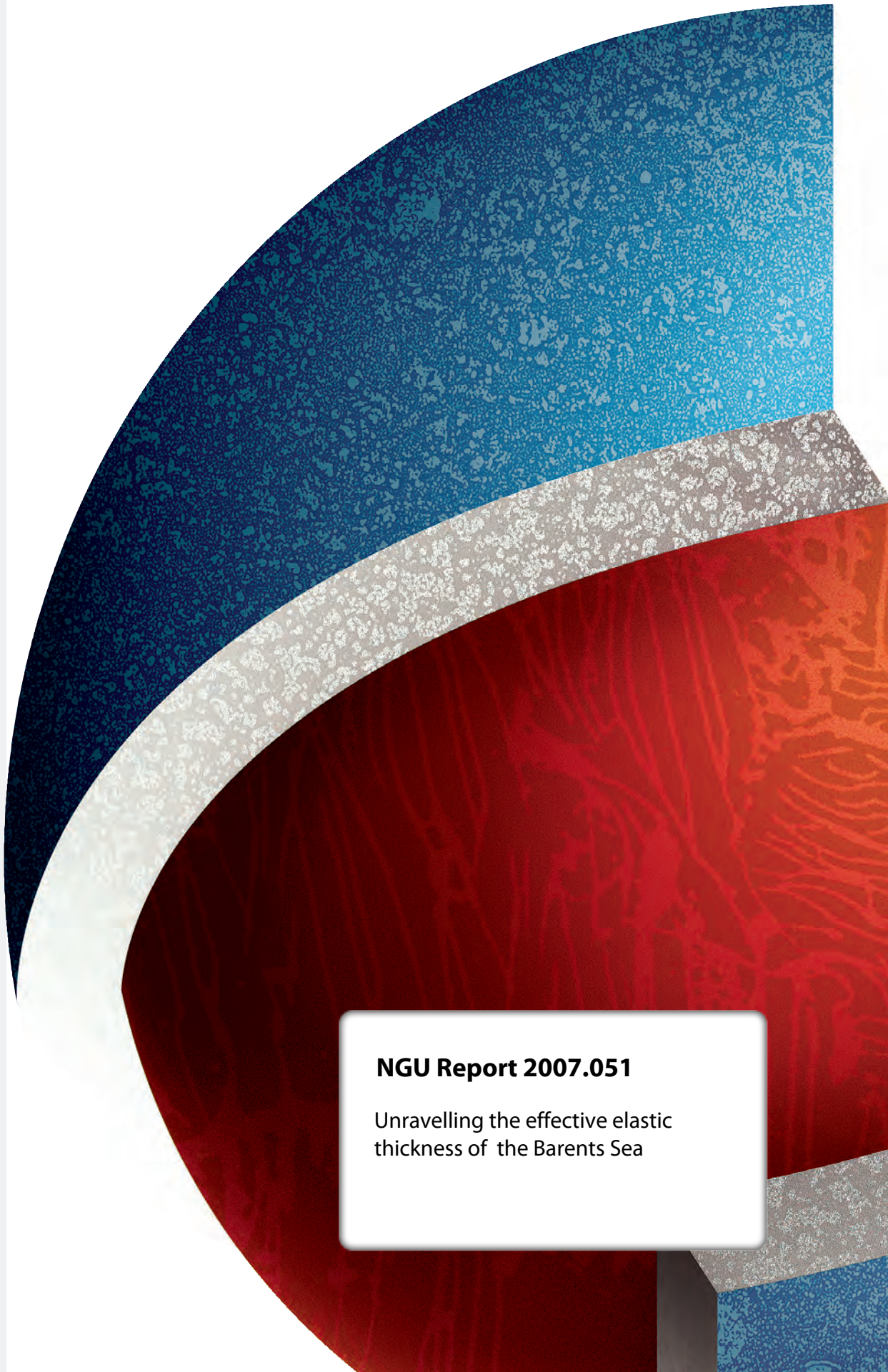

NGU Report 2007.051

Unravelling the effective elastic thickness of the Barents Sea

Geological Survey of Norway
NO-7441 Trondheim, Norway
Tel.: 47 73 90 40 00
Telefax 47 73 92 16 20

REPORT

Report no.: 2007.051 | ISSN 0800-3416 | Grading: Confidential until 31.12.2009

Title:
Unravelling the effective elastic thickness of the Barents Sea

Authors:
Susanne Buiter

Client:
StatoilHydro

County:

Commune:

Map-sheet name (M=1:250.000)

Map-sheet no. and -name (M=1:50.000)

Deposit name and grid-reference:

Number of pages: 33 Price (NOK):
Map enclosures:

Fieldwork carried out:

Date of report:
01.11.2007

Project no.:
313300

Person responsible:

Summary:

The Barents Sea area is characterised by deep sedimentary basins and a relatively flat-lying crust-mantle interface. The load of such sedimentary basins is generally compensated by the strength of the crust and lithosphere. A parameterisation of this strength can be obtained by considering the effective elastic thickness. I evaluate the effective elastic thickness of the Barents Sea region by forward calculation of lithospheric flexure under the loads of sedimentary layers and water. The effective elastic thickness is calculated along two profiles from south of Svalbard to Novaya Zemlya. I consider the following compensation mechanisms: 1) local compensation by Airy isostasy, 2) flexure of an elastic plate and 3) flexure of crust and lithosphere with a depth-dependent rheology. The results show that the present-day loads of water and sediments in the Barents Sea region are almost entirely compensated by local Airy isostasy or a very thin elastic plate. The crust of the Barents Sea is therefore weak from an isostatic point of view. The difference in width and depth of sedimentary basins between the western and eastern Barents Sea is not reflected in a difference in effective elastic thickness. I also find that lateral variations in effective elastic thickness are not needed to explain the main features of the basement deflection. This conclusion contrasts with Wienecke et al. (2007) who show low values for elastic thickness in the western Barents Sea and high values throughout the middle and eastern Barents Sea. Their high values may be a result of additional loads that were erroneously assigned to the crust and which require a higher plate strength for compensation. I show that the Wienecke et al. (2007) solution is too stiff and that their effective elastic thickness leads to a poorer fit to basement deflection than obtained in this report.

Keywords:	Barents Sea	Numerical modelling
Elastic thickness	Rheology	Flexure

CONTENTS

1. INTRODUCTION

The Barents Sea area was shaped during several phases of compression and extension. These tectonic events affected the Barents Sea lithosphere and could have led to long-term changes in its mechanical and thermal structure. A first order approach to search for trends that may identify old orogenies or extensional phases utilises the effect of such long-term changes in lithosphere structure by examining effective elastic thickness (T_e) values. This report focuses on the information contained in the T_e values for the Barents Sea region. I use numerical forward models of lithosphere flexure to identify the main contributions to T_e and to examine the sensitivity to thermal and mechanical parameters.

Effective elastic thickness is a parameter that describes the response of the lithosphere to long-term loading. Its value gives an indication of the ability of the lithosphere to support loads, as in the classic example of downwards flexure of oceanic lithosphere under the load of volcanic seamounts such as the Hawaiian islands (section 4.3 in Watts, 2001). In oceanic domains, T_e is mainly determined by thermal age and can to a first order be found by the depth to the 450-600°C isotherm (Watts, 1978). Old and cold lithosphere is strong (high T_e) and will deflect with a long wavelength, while young and warm oceanic plates are weak (low T_e) and can show large amplitude deflection with a short wavelength. In continents, T_e is determined by a combination of parameters. It reflects the integrated strength of the lithosphere, with contributions from elastic, viscous and brittle parameters (Burov and Diament, 1995; Watts and Burov, 2003). The Barents Sea region consists mainly of thinned continental lithosphere and the interpretation of its T_e is, therefore, not straightforward. My aim is to evaluate the effective elastic thickness of the Barents Sea region by forward calculation of lithospheric flexure under the loads of sediments and water. I present effective elastic thickness values along two east-west profiles through the Barents Sea. The results give information on depth-dependent stresses and the distribution of strong and weak layers with depth.

2. BRIEF SUMMARY OF THE REGIONAL SETTING OF THE BARENTS SEA

The Barents Sea is surrounded by Northern Norway, Northwest Russia, Novaya Zemlya, Franz Josef Land and Svalbard (Fig. 2.1). Its crust is continental, though thinned, and transits towards oceanic crust just west of Svalbard (Ritzmann et al., 2007). The region contains several structural highs and deep sedimentary basins. The Barents Sea area experienced several phases of compression and extension. During the Timanian orogeny (Late Precambrian), the Barents Sea, Novaya Zemlya and possibly Franz Josef Land amalgamated with Baltica. Along the eastern margin of Baltica, Ordovician-Silurian rifting opened the Uralian Ocean. This extension probably affected the North and South Barents basins just west of Novaya Zemlya (O'Leary et al., 2004). Closure of the ocean in the Uralian orogeny (Late Carboniferous-Early Permian) may have led to compressional structures as far north as Novaya Zemlya. The Pechora Basin is likely affected by foreland basin subsidence related to the Uralian orogen, but this signal is not clear in the basins west of Novaya Zemlya (O'Leary et al., 2004). These basins could have formed in multiple phases of extension (from the Ordovician to Early Triassic) (Otto and Bailey, 1995; Johansen et al., 1993; O'Leary et al., 2004), though large-scale normal faults are absent. A brief compressional episode, related to westward movement of Novaya Zemlya in the Late Triassic to Early Jurassic, mildly inverted the eastern Barents Sea basins (Otto and Bailey, 1995; Buiter and Torsvik, 2007).

The eastern margin of Greenland and the western margin of Norway collided in the Caledonian orogeny (Late Silurian). It is speculated that Caledonian trends are visible in the western Barents Sea, though the location of the Caledonian suture north of Norway is uncertain (Breivik et al., 2005; Cocks and Torsvik, 2005; Ritzmann and Faleide, 2007). The basins in the western Barents Sea formed by several extensional episodes during the Late Mesozoic, related to rifting of the North Atlantic, and Early Tertiary, related to extension and opening of the Norwegian-Greenland Sea (Faleide et al., 1993). The basins in the western Barents Sea are smaller and slightly less deep than the basins in the eastern Barents Sea.

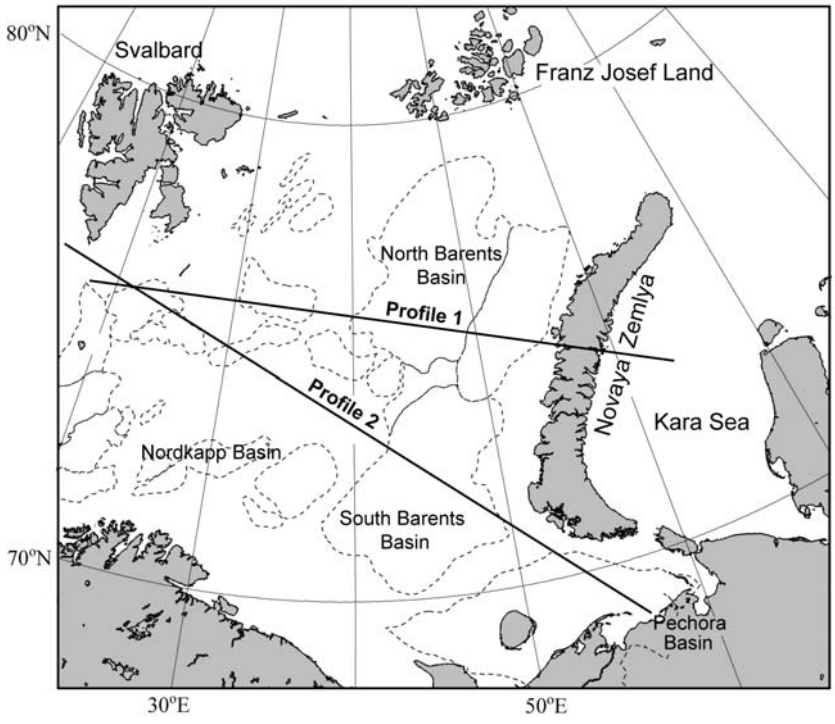

Fig. 2.1 Map of the Barents Sea area with the location of the two profiles investigated in this study. Modified after Buiter and Torsvik (2007).

3. FORWARD CALCULATION OF EFFECTIVE ELASTIC THICKNESS

3.1 Modelling method

The deflection of a lithospheric plate under loads can be approximated by the one-dimensional flexure equation (see also Turcotte and Schubert, 2002, Chapter 3):

$$\frac{d^2}{dx^2} D_e(x) \frac{d^2 w(x)}{dx^2} - P \frac{d^2 w(x)}{dx^2} + (\rho_m - \rho_o) g w = q(x) \qquad (3.1)$$

Here D_e is flexural rigidity, *w(x)* vertical deflection, *P* horizontal force, ρ_m and ρ_o density of material below and overlying the plate, respectively, *g* gravitational acceleration and *q(x)* the vertical load. I will neglect horizontal forces in this report (P = 0). The equation is valid for the following assumptions: 1) the plate is thin compared to its width, 2) the deflection is small compared to the width of the plate, 3) the deflection is plane strain, 4) the principal stress normal to the surface of the plate is zero, and 5) plane sections of the plate remain plane. The value of the effective flexural rigidity D_e is determined by the effective elastic thickness T_e and two elasticity parameters, usually Young's modulus *E* and Poisson ratio ν:

$$D_e = \frac{E T_e^3}{12(1-\nu^2)} \qquad (3.2)$$

D_e is easily calculated for a purely elastic plate. In continental lithosphere, however, effective elastic thickness does not correspond to a physical depth. It is instead a parameter with which continental flexural behaviour can be characterised. The value of D_e contains contributions from elastic and non-elastic components in material behaviour.

An effective flexural rigidity can be calculated by requiring that the bending moment supported by a plate with a continental rheology equals the bending moment of an elastic plate (Goetze and Evans, 1979; McNutt et al., 1988):

$$\int_{-h/2}^{h/2} (\sigma_{xx} - \sigma_{zz}) z dz = - D_e \frac{d^2 w}{dx^2} \qquad (3.3)$$

Here σ_{xx} and σ_{zz} are depth-dependent horizontal and vertical stress, respectively, d^2w/dx^2 is curvature and *h* is lithosphere thickness.

The distribution of lithosphere stress with depth depends on rheology. Figure 3.1 shows the stresses with depth for the example of a plate bending upwards, with tension at its top and compression at its base. The stresses in an elastic plate vary linearly with depth (Fig. 3.1a), but tend to get unrealistically high at the top and bottom of the plate. A cut-off on the maximum stress that can be sustained leads to an elastic-plastic rheology (Fig. 3.1b) (McAdoo et al., 1978). In the case of a visco-elasto-plastic rheology stresses are limited by brittle behaviour near the surface and ductile flow at the base (Fig. 3.1c). The maximum stress that can be supported is now determined by temperature (and thus heat production, surface heat flow and thermal conductivity), thickness of crust and lithosphere, composition, density, strain-rate and tectonic loading (tension or compression).

I calculate the present-day effective elastic rigidity for two profiles across the Barents Sea by iteratively solving the flexural equation (equation 3.1) for (1) a completely elastic plate and (2) a plate with a depth-dependent rheology (cf. Fig. 3.1c) (Appendix A). The equations are solved using a finite-difference method (Buiter et al., 1998; Buiter, 2000).

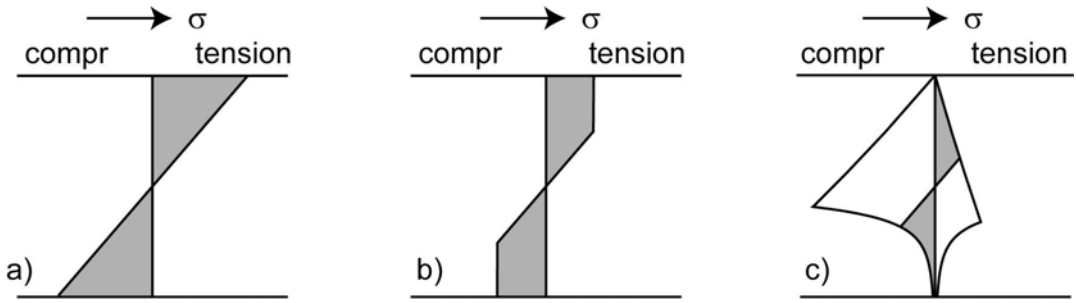

Fig. 3.1: The stress distribution ($\sigma = \sigma_{xx} - \sigma_{zz}$) in a flexing plate depends on rheology. This figure shows schematic examples for convex bending for (a) elastic, (b) elasto-plastic and (c) visco-elasto-plastic rheologies.

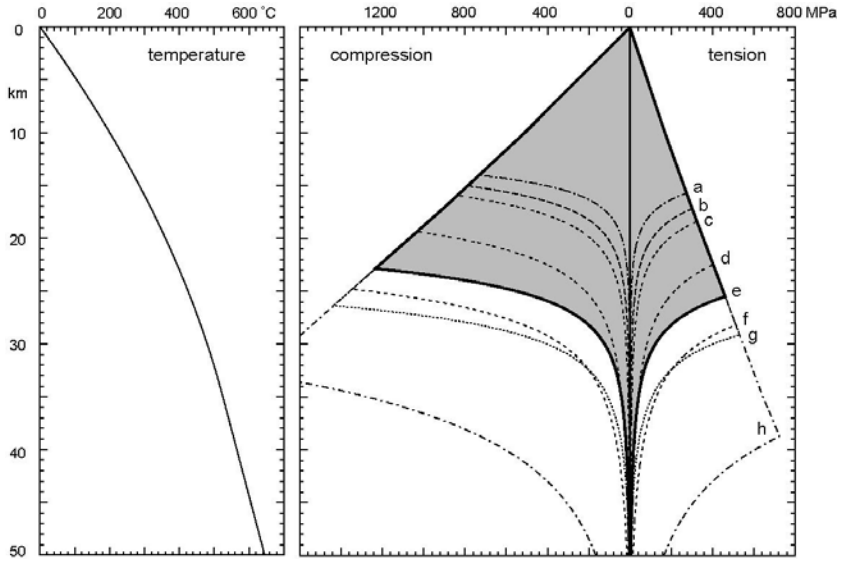

Fig. 3.2: Example of variations in crustal rheology. The yield envelope is calculated using a strain-rate of 10^{-15} s^{-1}, the values in Table 3.1 and the geotherm shown on the left, which is calculated following Chapman (1986). Flow laws: a) wet diorite (Hansen and Carter, 1982), b) Adirondack granulite (Wilks and Carter, 1990), c) dry anorthosite (Shelton and Tullis, 1981), d) wet diabase (Shelton and Tullis, 1981), e) wet anorthite (Rybacki and Dresen, 2000), f) Pikwitonei granulite (Wilks and Carter, 1990), g) microgabbro (Wilks and Carter, 1990), h) dry Maryland diabase (Mackwell et al., 1998). The bold line around the grey area (curve e) is the reference yield envelope used in the calculations for the Barents Sea. It is characterised by brittle behaviour until around 20-25 km depth below which ductile creep occurs.

The depth-dependent rheology is characterised by a yield envelope that gives the maximum stresses that can be supported. For stresses larger than the yield stress the rocks will fail by brittle behaviour or by ductile creep flow (Appendix A). Brittle behaviour is determined by the coefficient of friction, cohesion and the pore fluid factor (Table 3.1). The onset of creep is determined by strain-rate, temperature and by the material under consideration. The flow laws for crustal and mantle rocks are derived under laboratory conditions and need to be extrapolated across several orders of magnitude to lower strain-rates. Figures 3.2 and 3.3 show that there is a considerable range in available flow laws. For the Barents Sea study, I have chosen flow laws that are intermediate in the range of flow laws. The creep strength of

the crust and mantle is affected by the rate of deformation and temperature (Fig. 3.4). Regions that have high deformation rates and/or low temperatures are stronger.

For high surface heat flow and/or weak lower crust material, the crust may decouple from the upper mantle, as in Figure 3.3. This causes a substantial reduction in the effective elastic thickness of the lithosphere (McNutt et al., 1988).

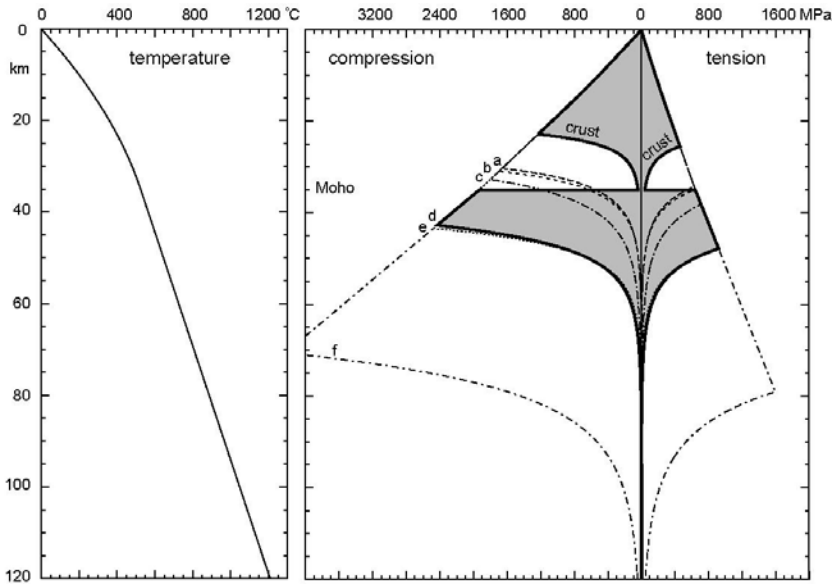

Fig. 3.3: Example of variations in mantle rheology. Parameter values as in Figure 3.2. Flow laws: a) wet Anita Bay dunite (Chopra and Paterson, 1981), b) wet olivine (Rutter and Brodie, 1988), c) wet Åheim dunite (Chopra and Paterson, 1981), d) dry olivine (Hirth and Kohlstedt, 1996), e) olivine (Goetze, 1978), f) dry dunite (Chopra and Paterson, 1984). The bold line around the grey area (curve d) is the reference yield envelope used in the calculations for the Barents Sea. It includes the crustal yield envelope for wet anorthite (Rybacki and Dresen, 2000).

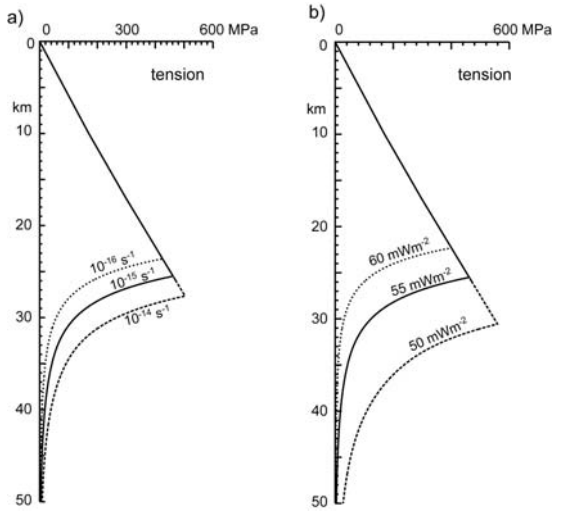

Fig. 3.4: Crustal creep strength depends on strain-rate and temperature (here parameterised with surface heat flow). The flow law is for wet anorthite (Rybacki and Dresen, 2000). In this study a strain-rate of 10^{-15} s^{-1} and a surface heat flow of 55 mW m^{-2} are used.

3.2 Mechanical and thermal parameters for the Barents Sea

The values of mechanical and thermal parameters used in the calculation of T_e for the Barents Sea are compiled in Table 3.1. The Moho depths are from Ritzmann et al. (2007). Along the two profiles investigated in this report, the Moho lies at 35 km depth on average. It is deeper (towards 50 km) under Novaya Zemlya and shallows westward towards the Greenland-Norwegian Sea. The sedimentary basins are deep, with an average depth of 10 km along both profiles (Ritzmann et al., 2007; Ivanova et al., 2006; Bungum et al., 2005). The density values for crust and sediments are from Ebbing et al. (2007). The sediment density ρ_s follows:

$$\rho_s(z) = \Phi_0 e^{-b_1 z}\rho_f + (1 - \Phi_0 e^{-b_2 z})\rho_r \qquad (3.4)$$

Here Φ_0 is initial porosity (0.6), ρ_f fluid density (1030 kg m^{-3}), ρ_r grain density (2700 kg m^{-3}) and b_1, b_2 are depth decay parameters ($b_1 = b_2 = 0.9$ km^{-1}). This results in an average sediment density of 2600 kg m^{-3} for a sediment thickness of 10 km. The surface heat flow is chosen at the relatively standard value of 55 mW m^{-2} for continental crust. Heat flow measurements in the Nordkapp Basin (not above salt diapirs) show similar values (Bugge et al., 2002).

Table 3.1 Model parameter values

Parameter	Symbol	Value
Moho depth		average 35 km
Density water	ρ_w	1030 kg m^{-3}
sediments	ρ_s	equation 3.4
crust	ρ_c	2900 kg m^{-3}
mantle	ρ_m	3300 kg m^{-3}
Strain-rate	$\dot{\varepsilon}$	10^{-15} s^{-1}
Gravitational acceleration	g	9.81 m s^{-2}
Friction coefficient	μ	0.577
Pore fluid factor	λ	0
Cohesion	C	0 Pa
Young's modulus	E	10^{11} Pa
Poisson's ratio	ν	0.25
Power law crust[1] pre-exponent	A	1.8 x 10^{-15} s^{-1} Pa^{-n}
activation energy	Q	356 kJ mole^{-1}
power	n	3.0
Power law mantle[2] pre-exponent	A	2.872 x 10^{-16} s^{-1} Pa^{-n}
activation energy	Q	535 kJ mole^{-1}
power	n	3.5
Thermal conductivity	k	2.5 W m^{-1} K^{-1}
Surface heat flow	Q_s	55 mW m^{-2}
Universal gas constant	R	8.31 J K^{-1} mole^{-1}
Heat production		10^{-6} W m^{-3}

[1] Rybacki and Dresen (2000)
[2] Hirth and Kohlstedt (1996)

4. PROFILE 1: MID-NOVAYA ZEMLYA TO SOUTH SVALBARD

Profile 1 runs from just south of Svalbard across the Barents Sea and the middle of Novaya Zemlya to the Kara Sea (Fig. 4.1, location in Fig. 2.1). It follows the profiles of Ivanova et al. (2006) and Bungum et al. (2005) (Fig. 4.2). The Ivanova profile shows a relatively flat-lying upper-lower crust boundary and Moho, without a substantial crustal root under Novaya Zemlya. The Bungum profile shows more pronounced differences in these horizons. In the calculations, I have used the sediment thickness and Moho depths from Ritzmann et al. (2007) on which the Bungum profile has been based. The upper crust and lower crust are combined in one layer. I calculate the deflection under the load of sediments and water and compare this to the depth of the basement. To avoid boundary effects, the profile is extended 1000 km on each side in the calculations.

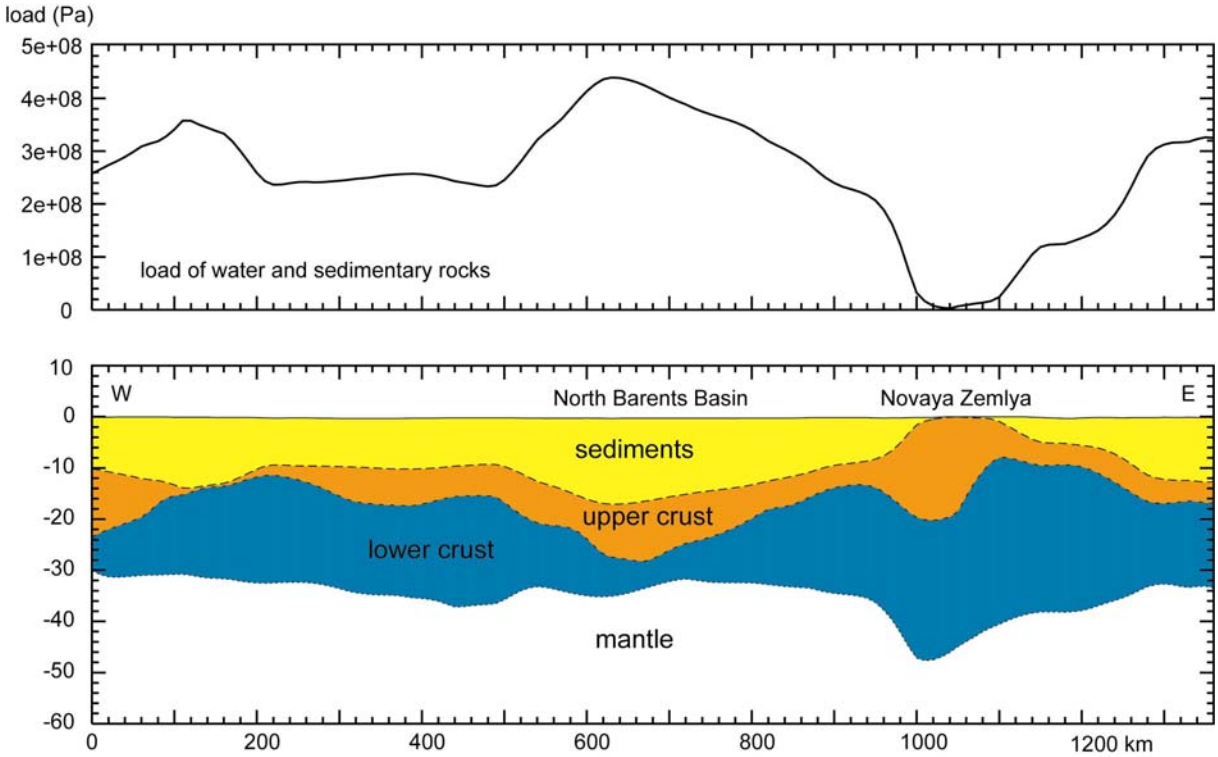

Fig. 4.1 (below) Thickness of the crust and sedimentary cover along profile 1 (see Fig. 2.1 for location), after Ritzmann et al. (2007) and (above) the vertical load exerted by the water and sediment layers.

4.1 Profile 1: Airy isostasy

Airy isostatic deflection of the basement, h_b, is calculated analytically from:

$$h_b(x) = \frac{\rho_w}{\rho_c}(h_w - h_w'(x)) + \frac{\rho_s}{\rho_c}(h_s - h_s'(x)) \qquad (4.1)$$

Here h_w and h_s are the reference values for water and sediment thickness, respectively (average values along the profile are used, with h_w = 195 m and h_s = 9899 m) and h'_w and h'_s are the actual water and sediment thickness along the profile. Along profile 1, the crust is almost in Airy isostatic equilibrium (Fig. 4.3). The good fit is a first indication that the crust along this profile is relatively weak. Differences between the Airy isostatic deflection and the basement depth can be seen below the basins and below Novaya Zemlya. The basement

subsidence is larger than the calculated deflection below the North Barents basin and the basin in the west Barents Sea, which could indicate that the crust or lithosphere contains additional loads in these regions. The calculated deflection does not reach the pronounced upward basement deflection observed at Novaya Zemlya.

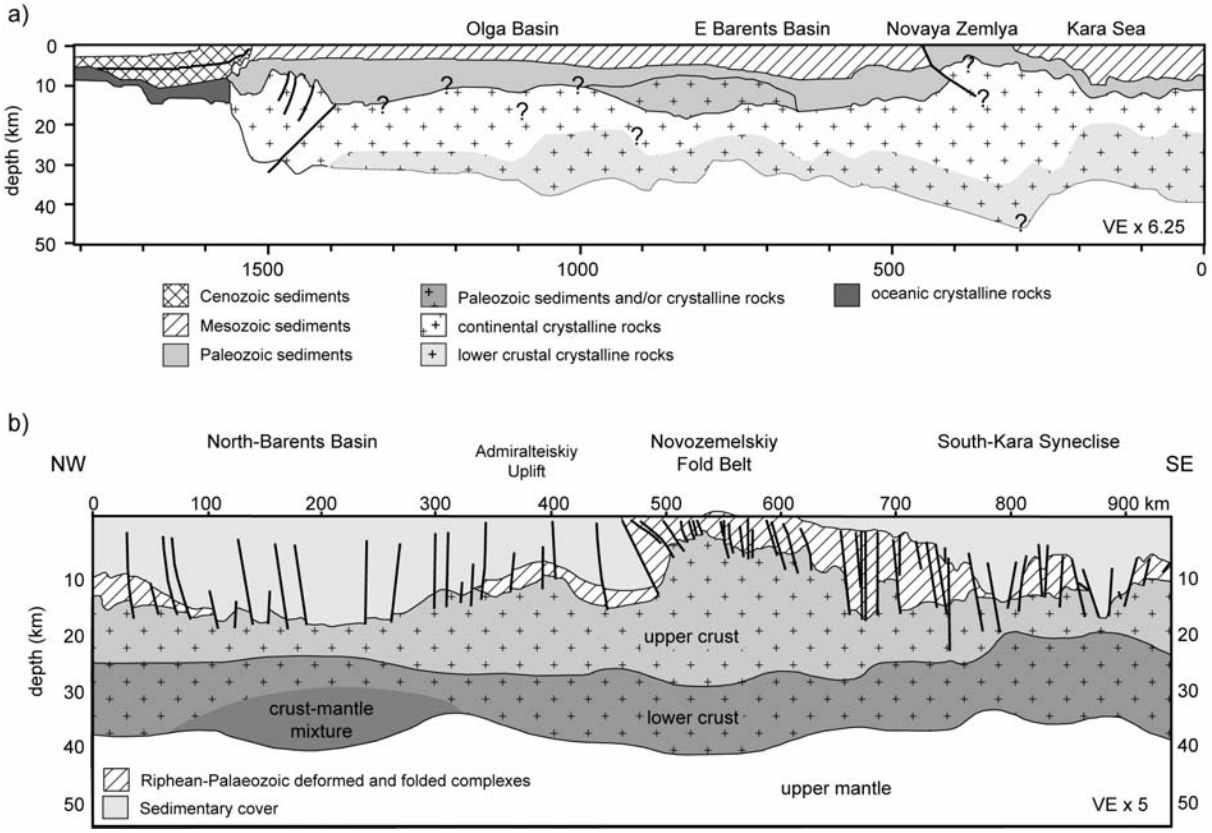

Fig. 4.2 Transects across the Barents Sea and Novaya Zemlya along Profile 1 indicated in Fig. 2.1. a) after Bungum et al. (2005). b) after Ivanova et al. (2006). Figure from Buiter and Torsvik (2007).

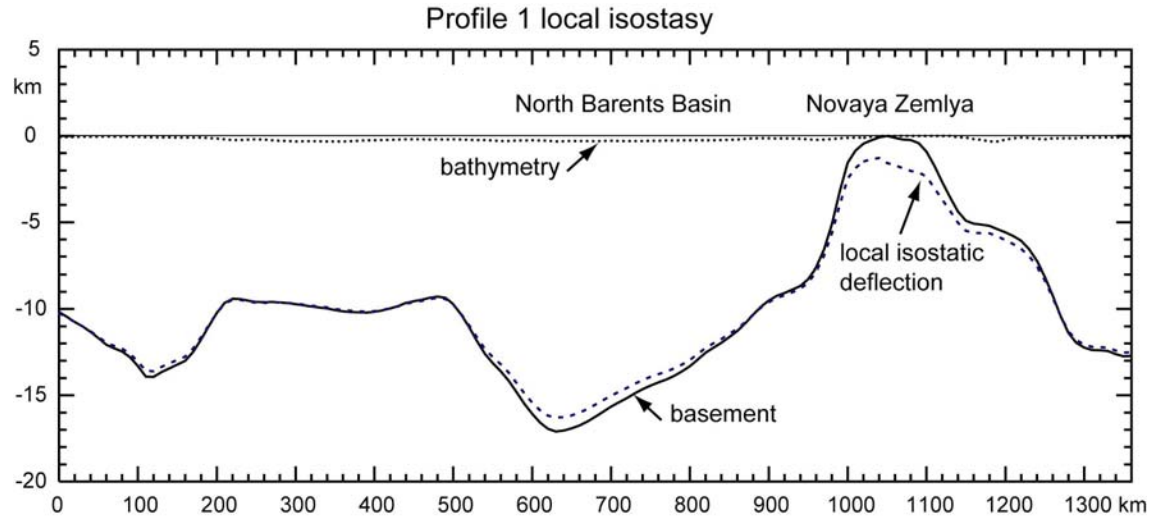

Fig. 4.3 Airy isostatic deflection compared to basement depth along profile 1. Density of mantle is 3300 kg m^{-3}, the sediment density has a constant value of 2600 kg m^{-3} (sediment density is depth-dependent in flexure calculations).

4.2 Profile 1: Elastic flexure

The deflection of a thin elastic plate is very similar to the Airy isostatic deflection. Figure 4.4a illustrates the flexural deflection for plates with low values of elastic thickness of 10 and 30 km. The fit to basement depth is again poor below the sedimentary basins and Novaya Zemlya. As expected, the elastic plate with a thickness of 30 km behaves stiffer than the plate with a thickness of 10 km. This can be seen most clearly in the regions where the curvature in the basement deflection is largest. Figure 4.4b shows the fit of flexure of a thin elastic plate to the Moho. The deflection is calculated by also including loads caused by density differences in the crust (using the density values of Ebbing et al., 2007) addition to the load of water and sediments. The fit for a low elastic thickness of 10 km is remarkably good.

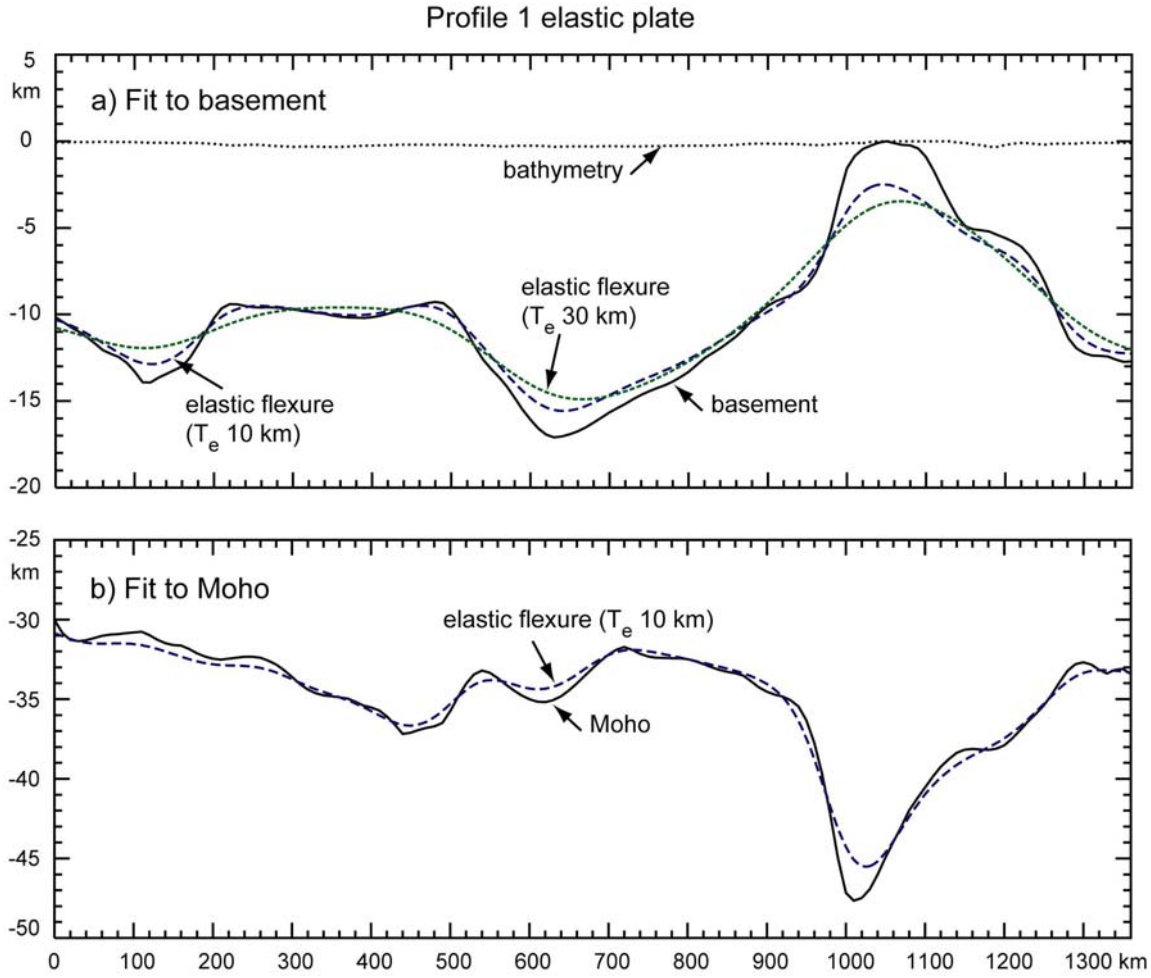

Fig. 4.4 Flexure of a thin elastic plate along profile 1. a) Deflection of plates with elastic thickness 10 and 30 km compared to basement depth. The elastic plate is loaded by water and sediments. b) Deflection of an elastic plate with thickness 10 km compared to the Moho. The plate is loaded by water, sediments and crustal density differences.

4.3 Profile 1: Crustal flexure

A plate with a single yield envelope rheology will have an effective elastic thickness equal to its mechanical thickness if no flexing occurs (and in absence of horizontal forces). The mechanical thickness is determined by the depth at which the stress has decreased to 50 MPa (Bodine et al., 1981) and is 32.4 km along profile 1 (average of the values in tension and compression, Appendix A). Figure 4.5a shows that this maximum is reached regularly along

the profile. The minimum is 13.9 km under Novaya Zemlya. The average T_e is 27.3 km. The deflection of a plate with a crustal rheology is very similar to the deflection of a homogeneous elastic plate with a thickness of 30 km (Fig. 4.5b). This is an indication that lateral variations in elastic thickness do not play an important role along this profile.

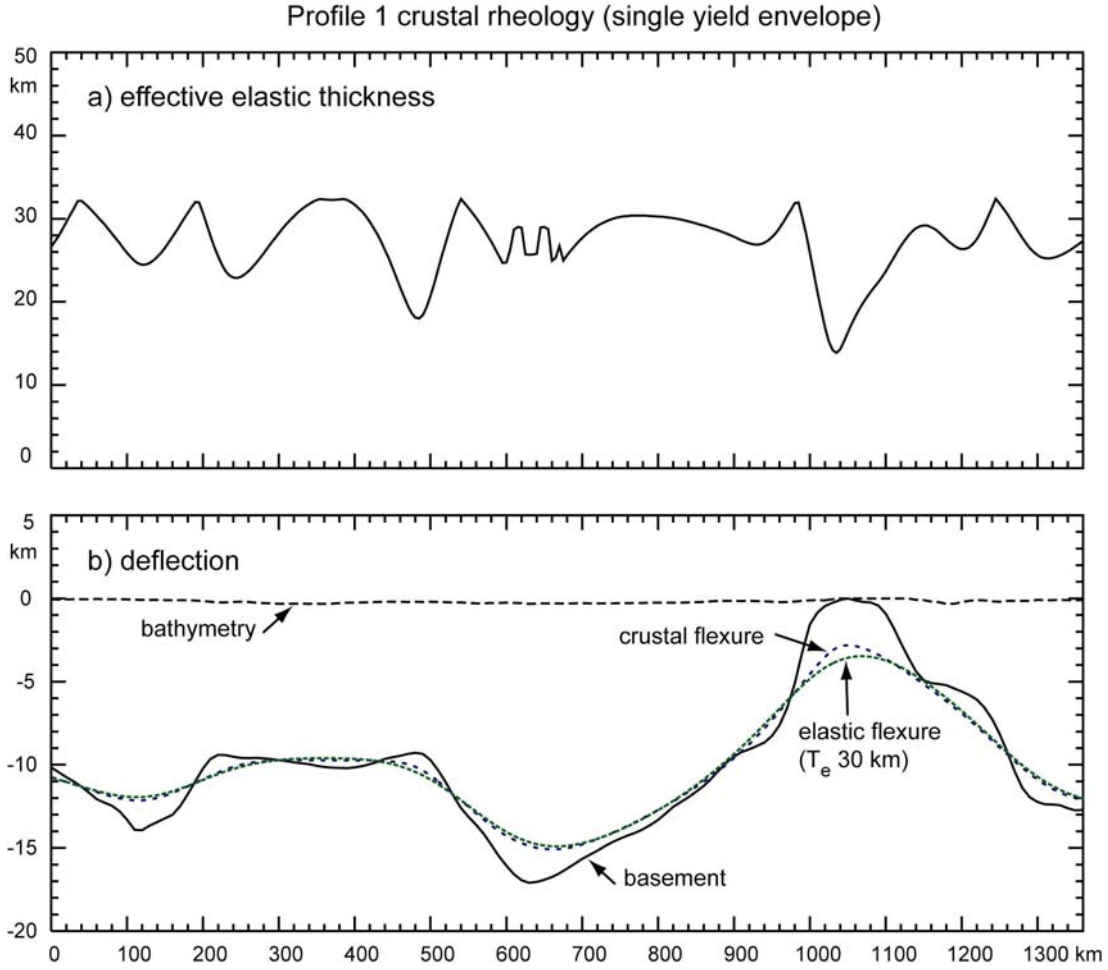

Fig. 4.5 Flexural deflection of a plate with a single yield envelope crustal rheology (Fig. 3.2) along profile 1. a) Effective elastic thickness. b) Calculated deflection (crustal flexure) compared with the deflection of an elastic plate (elastic flexure) and with the basement depth. Around x = 610-655 km wiggles in the T_e value indicate numerical difficulty in obtaining the solution at these locations.

The stress distribution with depth in Figure 4.6 shows that the top part of the plate behaves brittle, the middle elastic, while the bottom part fails by ductile creep. The thickness of the layer with elastic behaviour varies along the profile. Upward bending regions show tension at the top and compression at the base. This can be seen at the transition between the west and east Barents Sea basins at x=200-500 km. Downward bending causes compression at the top and tension at the base of the plate. This occurs in the North Barents Basin (x=600-900 km) (Fig. 4.6).

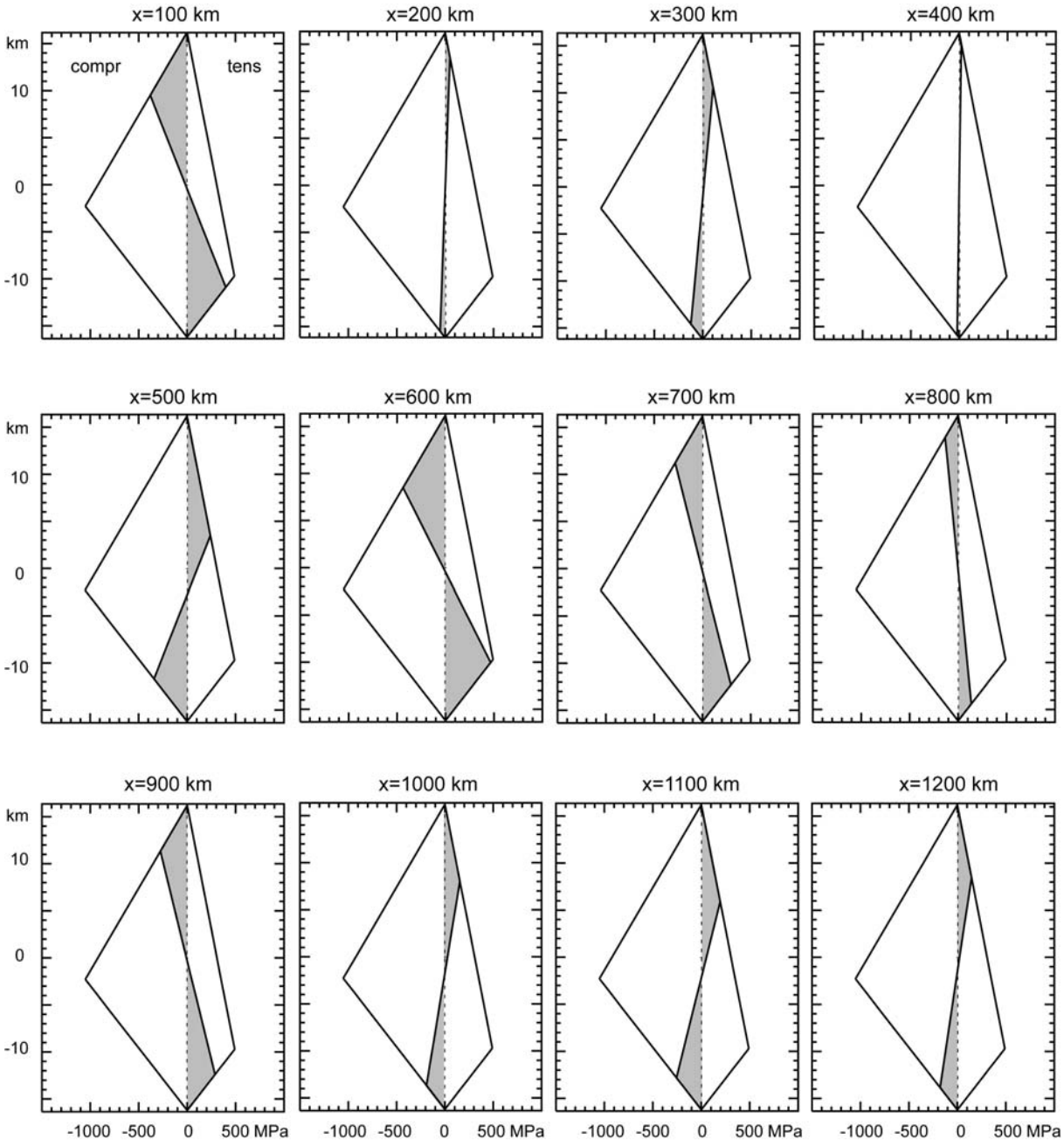

Fig. 4.6 Distribution of stress (σ_{xx}) with depth for selected locations along profile 1. This solution is for a single yield envelope crustal rheology (effective elastic thickness and deflection in Fig. 4.5).

The flow law for the lower crust in these calculations is for wet anorthite (Rybacki and Dresen, 2000) and has been chosen because it is intermediate in a range of lower crust flow laws. To test the sensitivity to the lower crust flow law, I have calculated T_e along profile 1 for a weaker (Adirondack granulite, Wilks and Carter, 1990) and a stronger rheology (microgabbro, Wilks and Carter, 1990) (Fig. 3.2). The weak flow law is characterised by a transition of brittle to ductile yielding between 10-12 km and a mechanical thickness of 22 km (average of compressional and tensile values). The weak lower crust is here obtained by using a weak flow law, but alternatively high temperatures (high surface heat flow) or low strain-rates would also result in a weak lower crust (Fig. 3.4). The strong flow law leads to a crust which is almost entirely brittle with a brittle-ductile transition between 25 and 30 km and a mechanical thickness of 36.6 km. The average T_e along Profile 1 is 18.4 km for the

weak rheology (Adirondack granulite), 27.3 km for the intermediate rheology (wet anorthite) and 31 km for the strong case (microgabbro) (Fig. 4.7a). These differences in T_e lead to only small differences in the flexural deflection (Fig. 4.7b).

In conclusion, the forward calculations of flexure of a plate with a crustal rheology show that the crust along profile 1 is relatively weak, that its effective elastic thickness lies between 20 and 30 km, and that lateral variations in T_e are not required to explain the basement deflection.

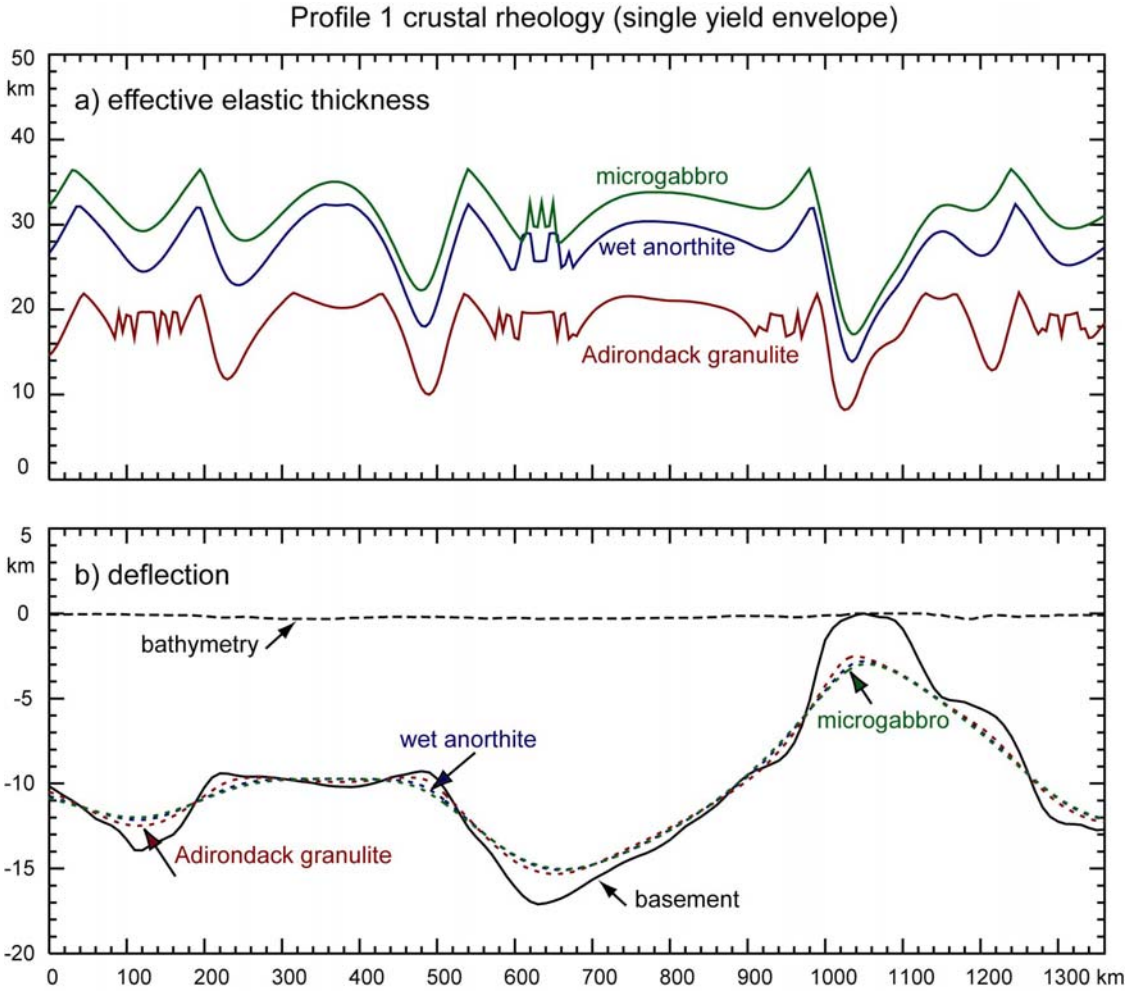

Fig 4.7 Sensitivity of crustal flexure to choice of flow law for creep behaviour in the lower crust. Wet anorthite (Rybacki and Dresen, 2000) is an intermediate flow law which has been used in the other calculations. Adirondack granulite is a weak flow law, while microgabbro is strong (both Wilks and Carter, 1990). A comparison of the strength profiles is shown in Figure 3.2.

4.4 Profile 1: Lithospheric flexure

Flexure of a plate with a lithospheric rheology, which includes yield envelopes in the crust and upper mantle, is shown in Figure 4.8. A plate with a double yield envelope rheology can have a high effective elastic thickness if the lower crust has a high enough strength to remain coupled to the upper mantle. As the Moho depth along profile 1 varies, coupling of crust and mantle occurs at x = 0-200 km and around x = 750 km along profile 1 (Figs. 4.8 and 4.9). If the lower crust decouples from the upper mantle, the effective elastic thickness is reduced (McNutt et al., 1988). This occurs in the remaining part of the profile. The average T_e is 38.5

km. If the high values (> 60 km) are ignored, the average T_e is 33.2 km, which is similar to the T_e of the plate with a crustal rheology. The high T_e values deteriorate the fit to the basement depth as the plate behaves too stiff in those regions (Fig. 4.8). Crustal flexure seems therefore to be more appropriate in this region. The stress distribution with depth shows again upward (convex) bending at the transition between the west and east Barents Sea basins (x = 300-500 km) and downward (concave) bending in the North Barents Basin (x=600-900 km) (Fig. 5.9).

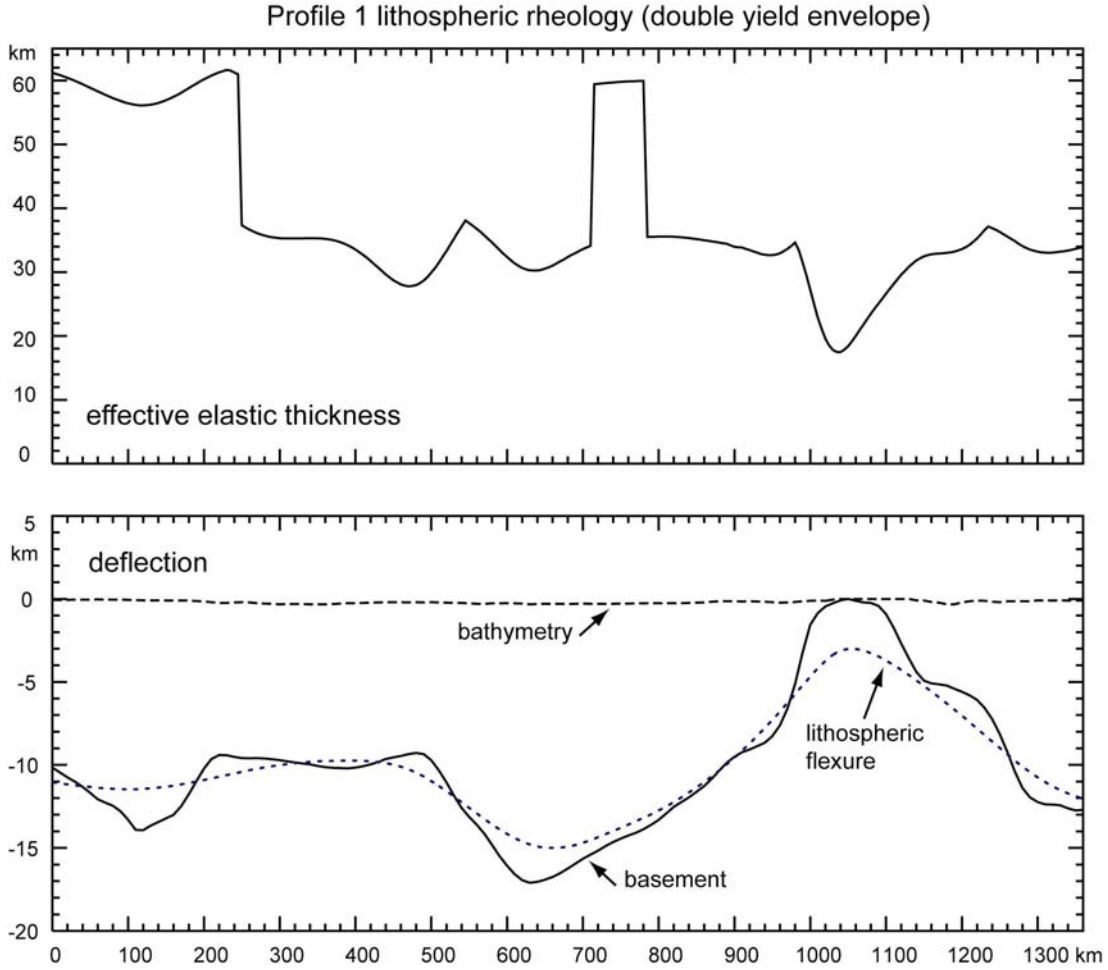

Fig. 4.8 Flexure of a lithospheric plate with a double yield envelope rheology (Fig. 3.3) along profile 1. The comparison to the basement depth is shown below, the effective thickness values are shown at the top. The mechanical thickness is 61.7 km

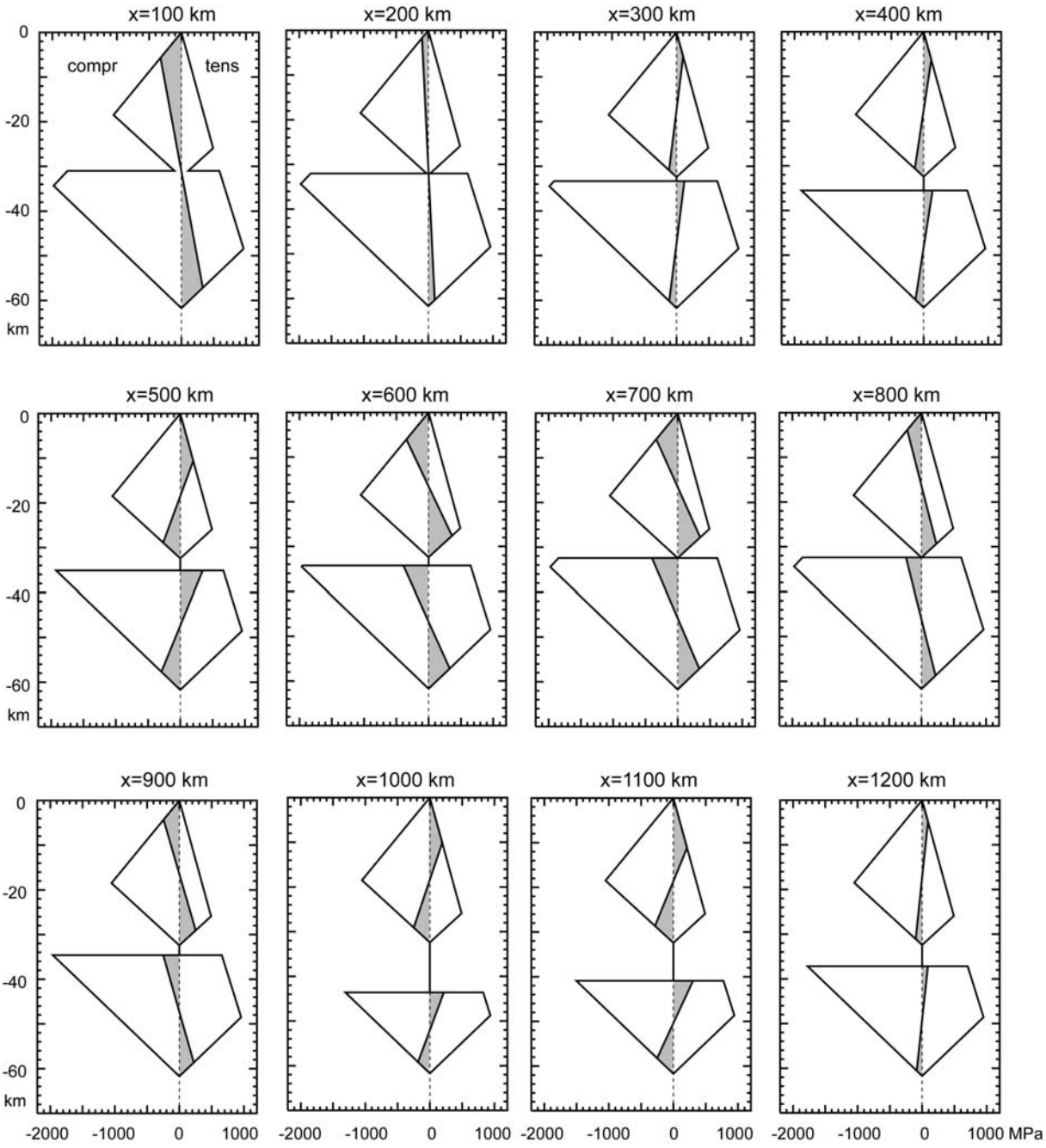

Fig. 4.9 Distribution of stress (σ_{xx}) with depth for selected locations along profile 1. This solution is for a double yield envelope lithospheric rheology (effective elastic thickness and deflection in Fig. 4.8).

5. PROFILE 2: SOUTH NOVAYA ZEMLYA TO SOUTH SVALBARD

Profile 2 lies to the south of profile 1 and runs from just south of Svalbard across the South Barents Basin to the Pechora Basin (Fig. 5.1, location in Fig. 2.1). The western part of the profile shows the transition to the oceanic crust of the Norwegian-Greenland Sea (for x < 200 km). Just east of this transition, the Moho is relatively flat and dips slightly to the east, increasing its depth from around 30 to 35 km. Near Novaya Zemlya (just to the north of the eastern part of the profile) the Moho becomes deeper. Around x=900-1000 km, west of the South Barents Basin, a remarkable thick basement is present. The origin of this basement block and the accuracy with which it is resolved in the Ritzmann et al. (2007) data is uncertain. In the following calculations, the basement and crust will therefore be treated as one layer. The profile is again extended 1000 km on each side.

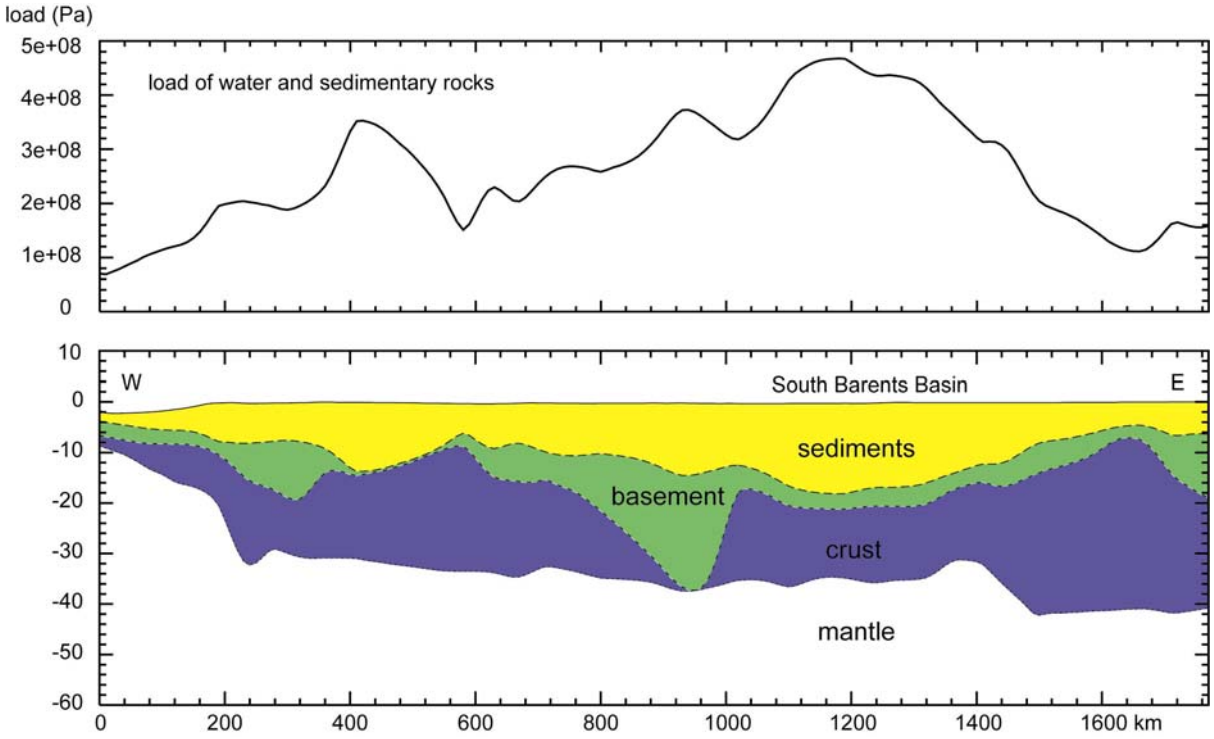

Fig. 5.1 (below) Thickness of the crust, basement and sedimentary cover along profile 2 (see Fig. 2.1 for location), after Ritzmann et al. (2007). The upper and lower crust are here combined in one layer. (above) The vertical load caused by the water and sediment layers.

5.1 Profile 2: Airy isostasy

The Airy isostatic deflection of the basement is calculated analytically by using equation 4.1 with an average water and sediment layer thickness of 330 m and 10070 m, respectively. Figure 5.2 shows that along profile 2, the load exerted by the layers of sediments and water on the Barents Sea crust is almost completely compensated by local Airy isostasy. Below the South Barents Basin, the calculated deflection is less than the basement deflection. This was also seen below the North Barents Basin along profile 1 (Fig. 4.3) and could be an indication of loads in the crust or mantle, or of sediments with a higher density than assumed.

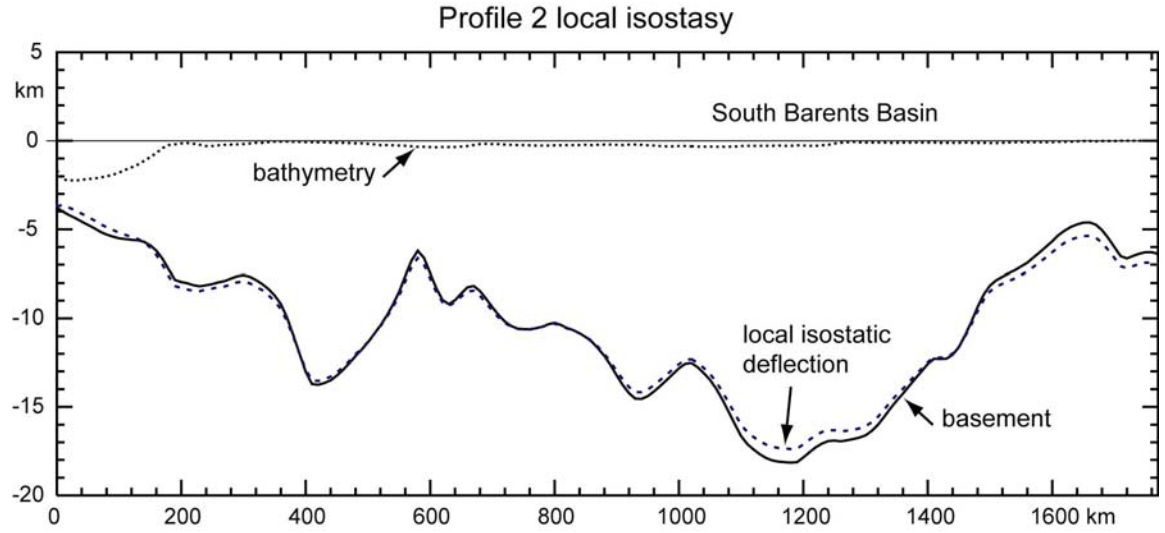

Fig. 5.2 Airy isostatic deflection compared to basement depth along profile 2.

5.2 Profile 2: Elastic flexure

The good fit to the basement deflection with Airy isostasy is an indication that the plate underlying the Barents Sea is rather weak. It is to be expected therefore that a thin elastic plate will also fit the basement deflection well and this is confirmed by the fit to basement of a plate with a thickness of 10 km in Figure 5.3. The deep deflection below the South Barents Basin is again not reproduced. A stronger plate (thickness 30 km) behaves stiffer and smoothens the basement undulations.

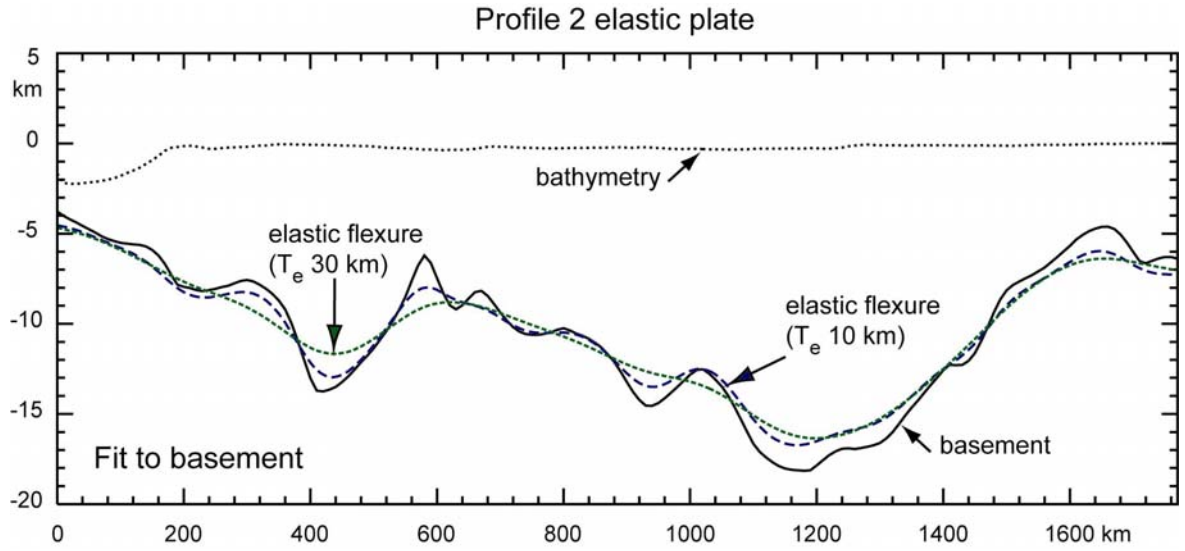

Fig. 5.3 Flexure of thin elastic plates (with thickness 10 and 30 km) along profile 2. The plates are loaded by water and sediments.

5.3 Profile 2: Crustal flexure

Flexure of the crust only is calculated by a single yield envelope rheology with a mechanical thickness of 32.4 km. The yield envelope is representative for continental crust and the oceanic domain (x < 200 km) is therefore not included in the model. The average effective

elastic thickness is 28.1 km, which is very similar to the average T_e of 27.3 km along profile 1. Low values (with a minimum of 15.7 km) occur where the curvature in the basement deflection is high, for example at x = 320, 580, 1020 and 1620 km. The maximum of 32.4 km is reached regularly along the profile (Fig. 5.4a). The deflection of the plate with a crustal rheology is again very similar to the flexure of a laterally homogeneous elastic plate with a thickness of 30 km.

The undulations of the basement cause lateral variations in convex and concave bending of the plate with resulting differences in the stress distribution with depth (Fig. 5.5). Beneath the South Barents Basin the plate bends downwards (concave bending) and the stress profiles show compression at the top and tension below (x=1100-1400 km in Fig 5.5).

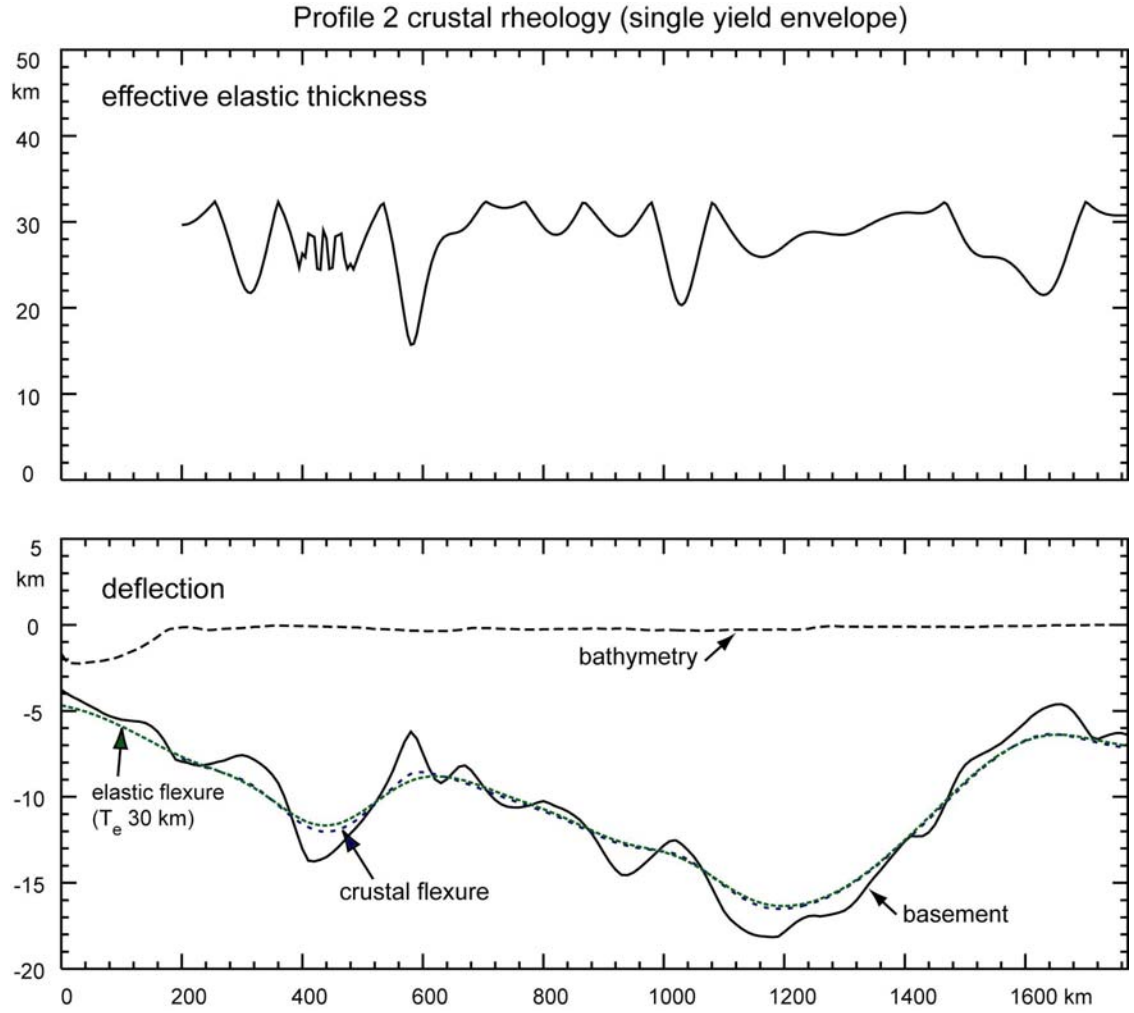

Fig. 5.4 Flexural deflection of a plate with a single yield envelope crustal rheology (Fig. 3.2) along profile 2. a) effective elastic thickness, b) calculated deflection (crustal flexure) compared with the deflection of an elastic plate (elastic flexure) and with the basement depth.

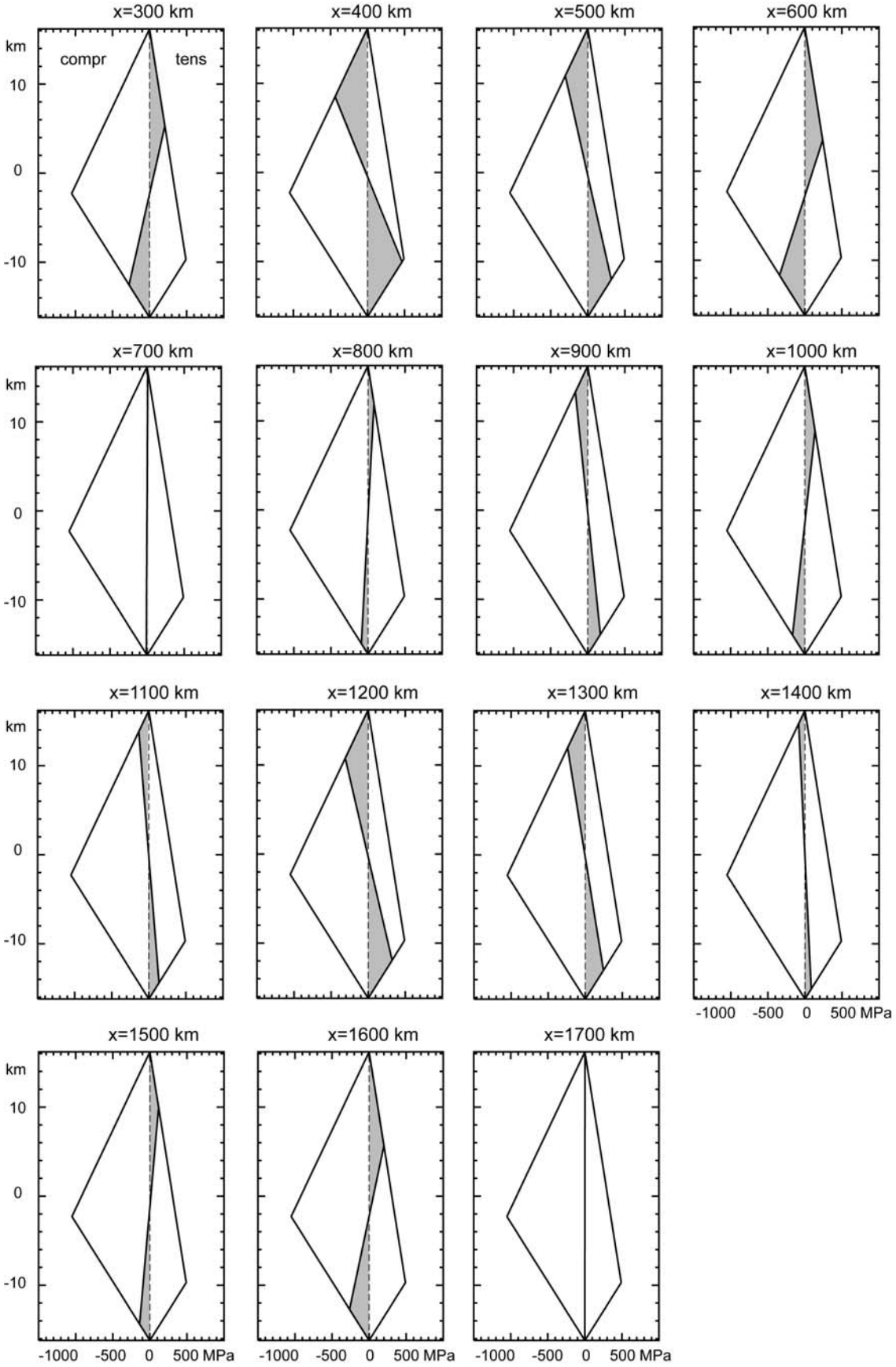

Fig. 5.5 Distribution of stress (σ_{xx}) with depth for selected locations along profile 2. This solution is for a single yield envelope crustal rheology (effective elastic thickness and deflection in Figure 5.4).

6. COMPARISON AND DISCUSSION OF THE TWO PROFILES

In this report, the effective elastic thickness is calculated along two west-east profiles in the Barents Sea: profile 1 from south of Svalbard across mid Novaya Zemlya and profile 2 from south of Svalbard to south of Novaya Zemlya. The T_e is obtained by simple numerical forward modelling of the basement flexural deflection under the loads of the present-day sediments and water layer. I have considered Airy isostasy, flexure of homogeneous elastic plates, crustal flexure and lithospheric flexure. In the last two cases, the crust and lithosphere have a depth-dependent rheology, which is characterised by brittle failure, elastic behaviour and ductile flow.

The results show that the loads of sediments and water in the Barents Sea area are almost entirely compensated locally by Airy isostasy or by a very thin elastic plate. This implies that the crust of the Barents Sea is weak from an isostatic point of view. The models do not show differences in flexural compensation behaviour between the two profiles or along the profiles. The difference in size and depth of the sedimentary basins between the west and east Barents Sea is thus not reflected in the (effective) elastic thickness values. Overall local compensation for the Barents Sea basins is also found by Ebbing et al. (2007) using local isostasy and forward density modelling. Their forward models, however, show that changes in the density distribution in the mantle are required between the west and east Barents Sea, which correlate with the overall change in basin configuration between the east and west Barents Sea. I find that the deflection of the basement is mainly a response to loading of the crust by sediments and that lateral changes in upper mantle density structure are not needed to explain the overall basement deflection. Lateral differences in T_e, which result from the depth-dependent rheology, do not play an important role and most of the flexural deflection can be explained by a laterally homogeneous thin elastic plate.

All flexural profiles of basement deflection in this report show local differences from the actual basement deflection. The sources of these local misfits could either lie in the basement depth data or in crustal loads that are not taken into account in the flexure calculations. The extremely thick basement block just west of the south Barents basin along profile 2 (between profile kilometre 900 and 1000, Fig. 5.1) may present an example of inaccuracies in the basement and crustal data. In some domains, the lower crust may have high seismic P-velocities (> 7 km s^{-1}) (e.g. Ivanova et al. 2006) and thus higher densities, resulting in an internal crustal load. Another source of internal loading may be related to intrusions in the crust (Ebbing et al., 2007).

7. COMPARISON TO THE ANALYTICAL SOLUTION OF AN ELASTIC PLATE

7.1 T_e obtained with forward modelling and inversion

In this report, I have used forward modelling of deflection data to obtain the effective elastic thickness along profiles. The effective elastic thickness of an area can also be calculated by inversion of topographic and gravity data. These two independent methods predict the same quantity (T_e) and their results should be approximately similar (see also Watts and Burov, 2003).

Wienecke et al. (2007) calculated the effective elastic thickness of the Barents Sea area using an inversion technique based on an analytical solution for an elastic plate (ASEP) (Fig. 7.1). Their solution is characterised by relatively high effective elastic thickness values (up to 65 km), with lower values (10-20 km) in the western part of the Barents Sea and underneath Novaya Zemlya. In contrast, my forward flexure models predict that the Barents Sea domain is in local Airy isostatic equilibrium or has low elastic thickness values (30 km or lower). The differences in the results of the two methods are substantial and imply that the Barents Sea is considered isostatically strong from the point of view of the results of Wienecke et al. (2007) and weak based on the results presented in this report.

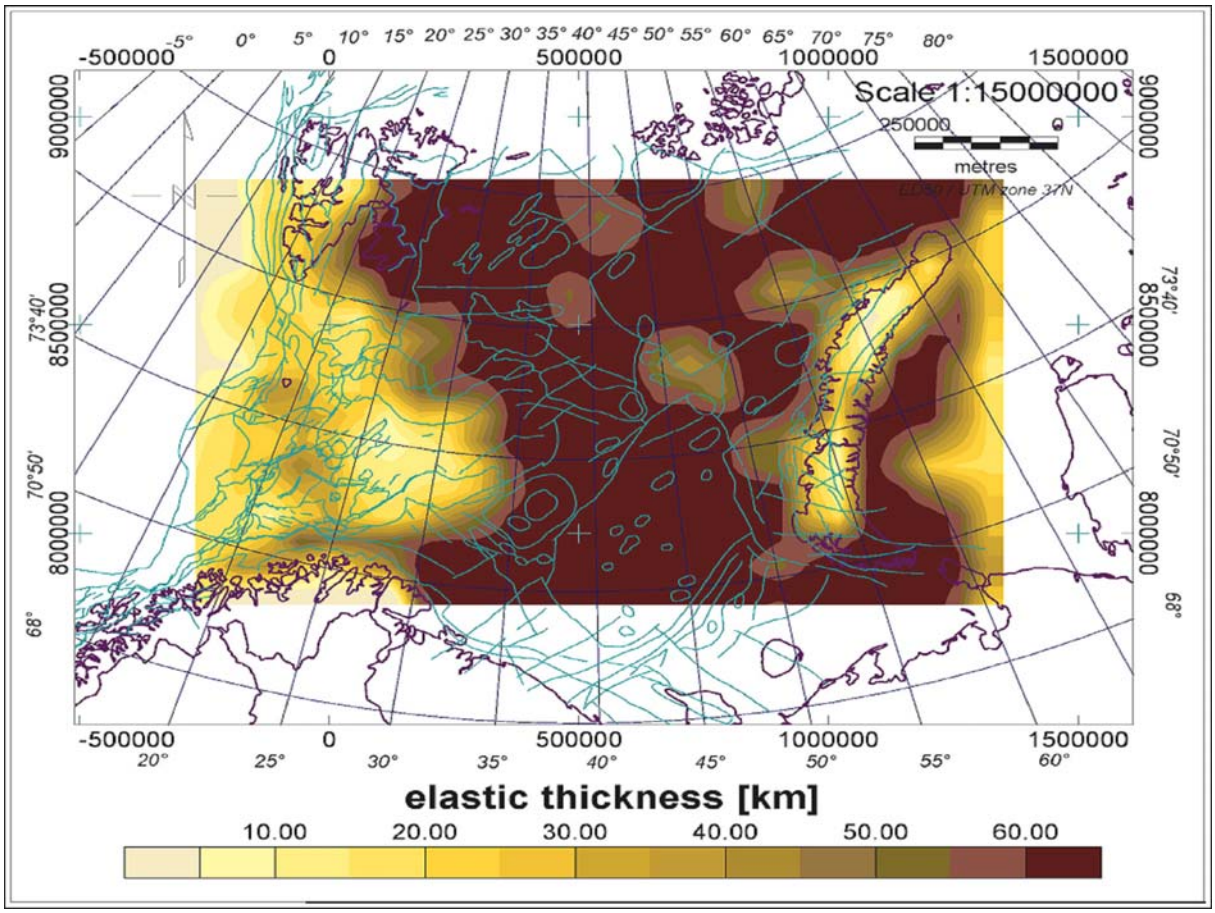

Fig. 7.1: Map of effective elastic thickness of the Barents Sea from Wienecke et al. (2007), calculated using the analytical solution for an elastic plate (ASEP).

Additional tests have therefore been performed to attempt to constrain the causes of the differences in the results obtained with the two methods.

7.2 Tests of modelling methods

The first test considers loading of an elastic plate with a laterally varying thickness (Fig. 7.2). A symmetric topographic load is centred close to a change in elastic thickness from 25 to 10 km. This causes a deflection which is slightly asymmetric. The topography of the load is held fixed and the area between the load and the deflection it causes is considered to be filled with the same loading material. The final load is therefore around 21 km high. This approach requires an iterative solution, since the deflection is not known beforehand. Figure 7.2 shows that the results from the forward method used in this report and the analytical solution for an elastic plate (ASEP) used in the inversion are very similar. The test therefore confirms that the solution given by the two different methods is in principle the same.

The inversion technique fixes the topography of the load and adds material underneath to fill up the deflection. This is suitable for orogenic settings, where the topography is known and the material underneath less well constrained. The forward technique I use in this report can be used in the same manner (Fig. 7.2). Alternatively, it can apply a load of which the size is known without adding additional material. The latter approach is for example suitable for modelling the deflection caused by the loading by known water or sediment layers such as in the Barents Sea.

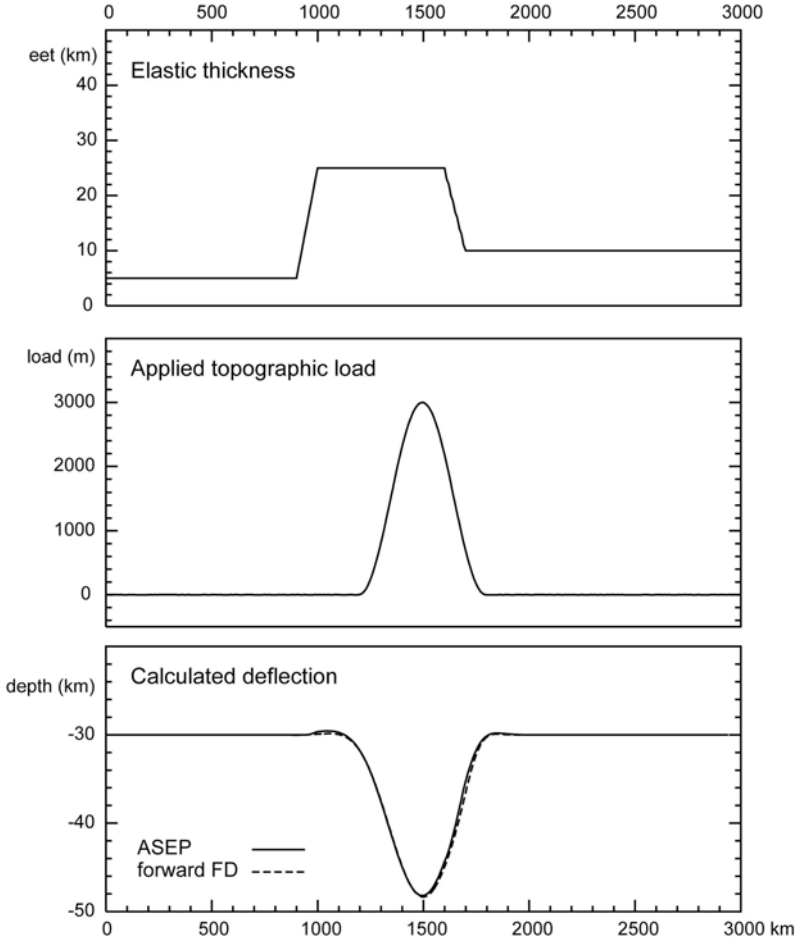

Parameter	Value
Topo density	2800 kg m^{-3}
Crust density	2800 kg m^{-3}
Mantle density	3200 kg m^{-3}
Young's modulus	10^{11} Pa
Poisson's ratio	0.25

Fig. 7.2 (left below) Comparison of flexural deflection calculated with the ASEP technique (as used in Wienecke et al. 2007; this calculation by Jörg Ebbing) to that calculated by solving the flexure equation with a finite difference technique (as used in this report). A plate of varying elastic thickness (left top) is loaded by a symmetric topographic load (left middle) that is fixed in height.

The synthetic model in Figure 7.2 is calculated in 2D for the forward method used in this report, but in 3D for the ASEP method. Using the load and the deflection, an inversion can be made for elastic thickness in the 3D model domain and compared with the original elastic thickness map. Figure 7.3 shows the elastic thickness obtained by the inversion superposed on the original elastic thickness. The 2D solution of Figure 7.2 is for y = 1500 km. The inversion reproduces the first order features of the synthetic model with low elastic thickness values on the sides and high values in the middle of the domain. Figure 7.3 also shows variations in elastic thickness, that are introduced by the inversion, but which are not present in the original synthetic model. These differences can be up to 20-25 km.

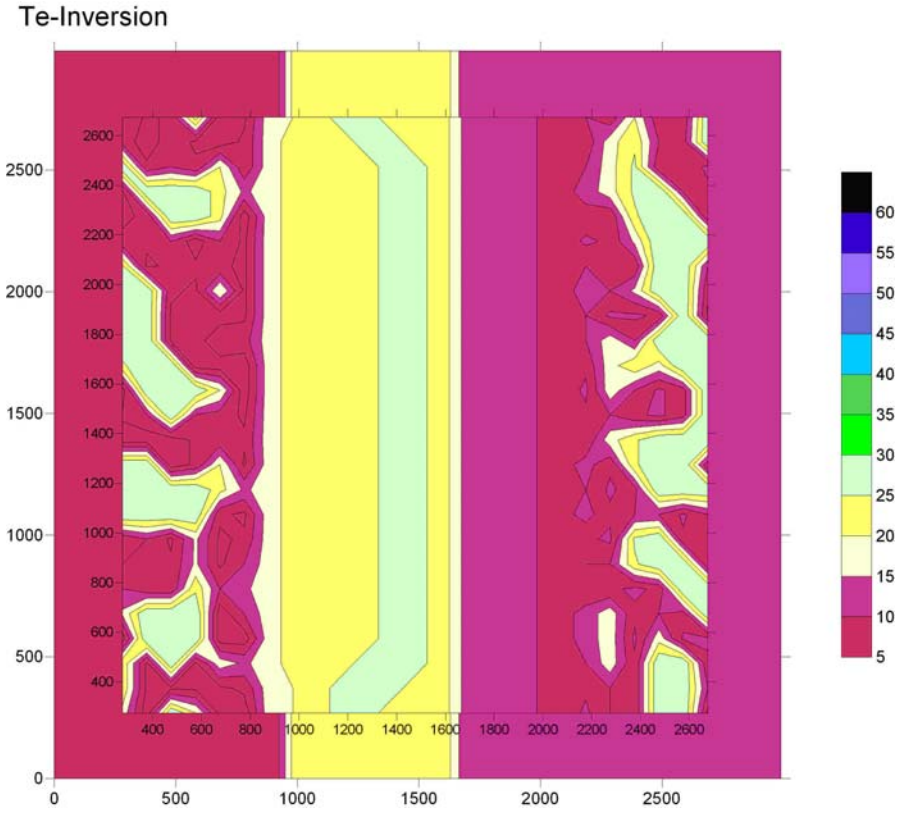

Fig. 7.3 Solution obtained by inversion (small domain) superposed on the initial T_e distribution. The colour scale-bar shows elastic thickness in km.

As a second test, I have calculated the deflection under the load of sediments and water along profile 1 using the Wienecke et al. (2007) effective elastic thickness. The T_e is read from their map (Fig. 7.1), because it could not be extrapolated digitally from their results. Figure 7.4 shows that the fit to basement using the Wienecke et al. (2007) T_e is worse than the fit of the deflection calculated with a laterally homogeneous thin elastic plate. In Figure 7.5 the fit of model flexure to the basement data is quantified using the root-mean-square (rms) difference:

$$\sqrt{\frac{1}{n}\sum_{n}\left(w_{flex}-w_{obs}\right)^2}$$

Here n is the number of measurents, w_{flex} the calculated deflection and w_{obs} the observed deflection. A lower value for an rms difference means that the fit is better. Figure 7.5 shows that the fit to basement deflection is best for low values of elastic thickness. The laterally

variable T_e of Wienecke et al. (2007) (Fig. 7.4a) along profile 1 is 47.6 km on average. The deflection calculated with the variable T_e of Wienecke et al. (2007) (Fig. 7.4) results in a fit which is better than that of a laterally homogeneous plate with a thickness of 47.6 km. However, a better fit would be obtained for a plate with a lower effective elastic thickness. The lithosphere of the Wienecke et al. (2007) solution is too stiff.

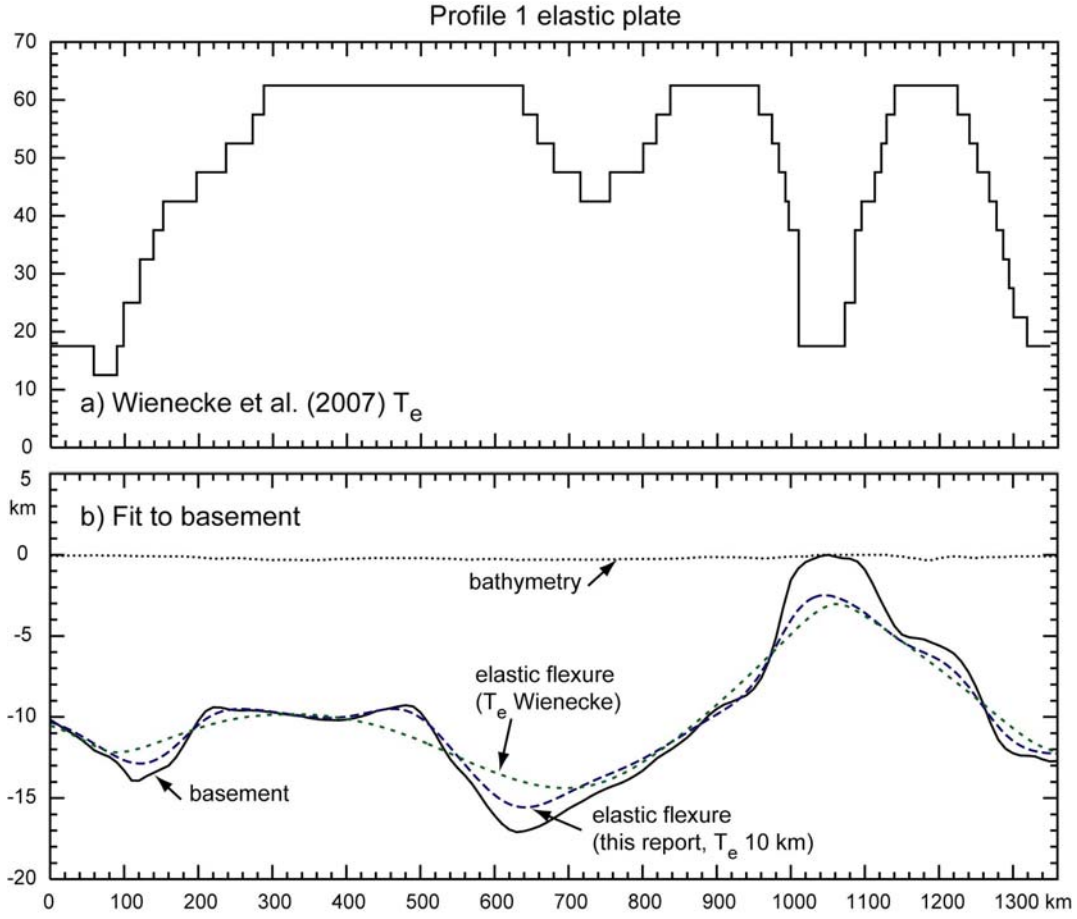

Fig. 7.4 a) Effective elastic thickness along profile 1 read from Wienecke et al. (2007) (Fig. 7.1). b) Flexure of a laterally homogeneous elastic plate of 10 km thickness leads to a better fit to basement than flexure calculated with the T_e of Wienecke et al. (2007).

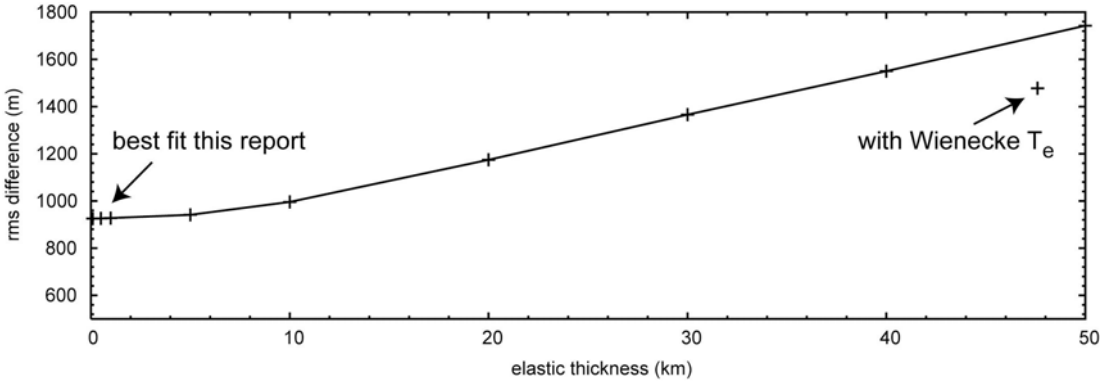

Fig. 7.5 Fit of calculated flexure to basement data quantified by rms-difference (low rms values denote a better fit) versus elastic plate thickness for profile 1. A low elastic thickness gives a good fit to basement deflection. Flexure calculated using the variable Wienecke et al. (2007) T_e gives a somewhat better fit than the flexure of a laterally homogeneous plate with 47.6 km thickness, but the fit of a thin elastic plate is better.

7.3 Conceptual differences in modelling methods

The synthetic test shows that the two modelling methods (forward finite difference of this study and ASEP of Wienecke et al., 2007) give the same solution to a simple problem. However, they result in different solutions for the Barents Sea area, with ASEP leading to higher values for the effective elastic thickness than the forward modelling method. A reverse test in which the T_e solution of ASEP is used in the forward modelling method shows that the ASEP solution is too stiff and does not results in a good fit to the Barents Sea basement deflection. It is here speculated that the ASEP solution may need such a stiff plate to compensate for additional loads that are applied. This points to a conceptual difference in the modelling techniques (Fig. 7.6).

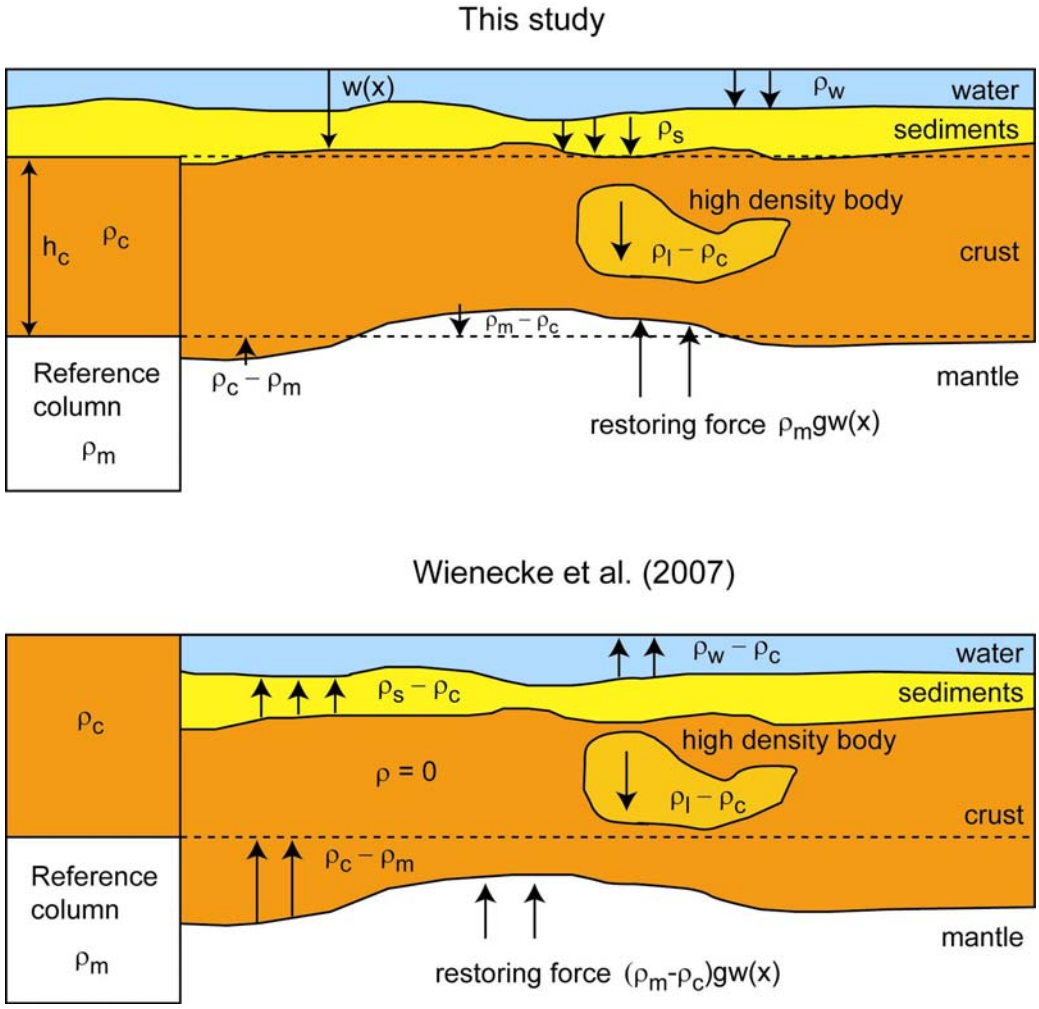

Fig. 7.6 (top) The forward model applied in this study uses the full load of the water and sediment layers to calculate the basement deflection. If used to calculate the deflection of the crust-mantle interface, the loads caused by lateral density and thickness changes in the crust are also taken into account. The crustal reference column then uses the average crustal thickness along the profile (e.g., h_c = 24.9 km along profile 1). (below) The ASEP method refers all densities, including those of the water and sediment layers, to a reference column. In the Barents Sea area a reference Moho depth of 30 km is used (Wienecke et al., 2007), which is less than the average Moho depth of the region.

In order to calculate the deflection of the crust-mantle interface, not only the loads of sediments and water, but also internal crustal loads and crustal thickness changes need to be

taken into account. To calculate the loads related to the crust, I use a crustal reference column that is obtained by averaging of the crustal thickness and densities along the profile under consideration. This means that both positive and negative loads will be present along the profile (Fig. 7.6 top). Wienecke et al. (2007) refer all layers, including the water and sediment layers, to a reference column (Fig. 7.6 bottom). Their reference Moho lies at 30 km depth. However, because the crust-mantle interface is on average deeper than 30 km in the Barents Sea area, this choice results in additional upward directed forces. These extra forces then need to be compensated by an increase in elastic thickness. This would explain the generally high T_e values of Wienecke et al. (2007). It would be interesting to see the solution that uses a reference depth which is more in line with the average Moho depth in the area, e.g., 35 km.

8. CONCLUSIONS

This study reports the effective elastic thickness (T_e) along two east-west profiles in the Barents Sea region, from south of Svalbard to Novaya Zemlya. The T_e is obtained by forward modelling of lithospheric flexure under the loads caused by sediment and water layers and by fitting the calculated flexure to the sediment-basement interface. I show the following:

1. The Barents Sea crust is isostatically weak along both profiles. This is shown by the best fits to the sediment-basement interface and the Moho obtained by local Airy isostasy or a very thin elastic plate.
2. There is no difference in T_e between the west and east Barents Sea along the profiles. The difference in size and depth of the sedimentary basins between the west and east is thus not reflected in a difference in T_e.
3. There is no indication of a Caledonian suture along the modelled profiles.
4. Crustal flexure with a depth-dependent rheology results in brittle, elastic and ductile material behaviour (from top downwards). The average effective elastic thickness along the two profiles is around 30 km for crustal flexure.
5. The water, sedimentary and crustal loads can be compensated by the crust. The lithosphere is not necessarily needed to compensate these loads.
6. The difference between the results reported in this study and Wienecke et al. (2007) could be caused by the introduction of artificial additional loads in Wienecke et al. (2007) related to their choice of a too shallow reference Moho.
7. A T_e of 48 km on average as obtained by Wienecke et al. (2007) is too stiff to explain the deflection of the sediment-basement interface.

Acknowledgements

I thank Jörg Ebbing for many discussions on flexural isostasy and for the calculations with the ASEP method for the synthetic model and inversion of section 7.2. Trond Torsvik is thanked for discussions on the tectonic history of the Barents Sea region. The research reported in this study was conducted in the project BASIC which was supported financially by Statoil ASA.

APPENDIX A: BRITTLE AND DUCTILE MATERIAL BEHAVIOUR

The maximum stress in the brittle regime follows the frictional criterion of Byerlee (1978):

$$\tau = \mu' \sigma_n + C \approx \mu \sigma_n \tag{A.1}$$

Here μ is the coefficient of friction, and τ and σ_n are the shear and normal stress acting on the surface under consideration. In terms of principal stresses σ_1 and σ_3 this becomes (Jaeger and Cook, 1979):

$$\begin{aligned} compression: (\sigma_1 - \sigma_3) &= \frac{2\mu}{\sqrt{1+\mu^2} - \mu} \rho g z (1-\lambda) \\ tension: (\sigma_1 - \sigma_3) &= \frac{2\mu}{\sqrt{1+\mu^2} + \mu} \rho g z (1-\lambda) \end{aligned} \tag{A.2}$$

Here ρ is rock density and λ the pore-fluid factor (pore-fluid pressure divided by lithostatic pressure). For small deflections typical for lithospheric flexure, the horizontal and vertical stress can be considered approximately equal to the principal stresses. Using that $\sigma_{zz} = 0$ for the flexural equation, Byerlee's law becomes:

$$\begin{aligned} compression: \sigma_{xx} &= \frac{2\mu}{\sqrt{1+\mu^2} - \mu} \rho g z (1-\lambda) \\ tension: \sigma_{xx} &= \frac{-2\mu}{\sqrt{1+\mu^2} + \mu} \rho g z (1-\lambda) \end{aligned} \tag{A.3}$$

At higher temperatures, power law creep takes over. The flow law generalised to effective stress is (Ranalli, 1987):

$$\dot{\varepsilon}_{ij} = A \sigma_E^{'(n-1)} \sigma_{ij}^{'} e^{\frac{-Q}{RT}} \tag{A.4}$$

Here $\dot{\varepsilon}_{ij}$ is the strain-rate tensor, T(x,z) temperature, R the universal gas constant, Q activation energy, n flow law power, A flow law pre-exponent, σ'_{ij} the deviatoric stress tensor and effective stress σ'_E is $(\sigma'_{ij}\sigma'_{ij}/2)^{1/2}$. Using the constraints of the flexural equation (equation 3.1) (plane strain, vertical stress is zero), the flow law can be rewritten to horizontal stress only:

$$\sigma_{xx} = \dot{\varepsilon}_{xx}^{1/n} A_m^{-1/n} e^{\frac{Q}{nRT}} \tag{A.5}$$

Where A_m is the modified flow law parameter.

Equations A.3 and A.5 define the depth-dependent yield stress. For stresses larger than the yield stress, the rocks will fail by brittle behaviour or by power law creep. In order to determined the effective flexural rigidity it is necessary to integrate the product of yield stress with depth over depth (equation 3.3). To facilitate this integration, the creep curves are fit to a linear line (Fig. A.1).

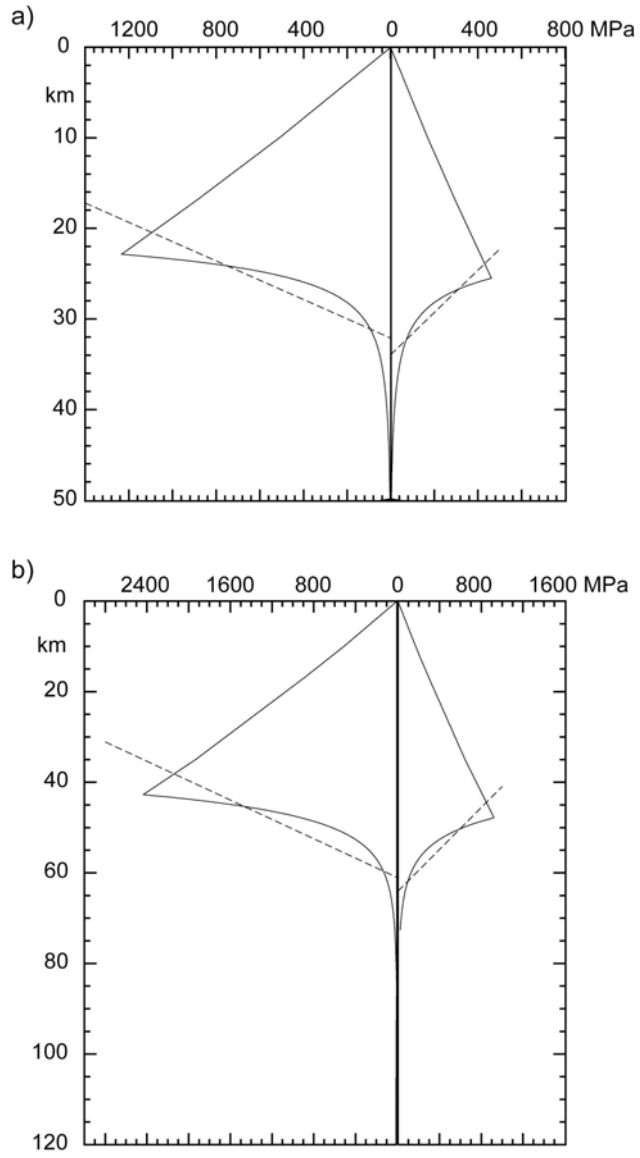

Fig. A.1 Linearised fit to power flow law. a) The crustal flow law for wet anorthite (Rybacki and Dresen, 2000) is fit by 1.039 x 10^5 Pa m^{-1} in compression and 4.74 x 10^4 Pa m^{-1} in tension. The mechanical thickness (defined by depth at which the stress is 50 MPa) is 31.5 and 33.3 km, respectively. b) The mantle flow law for dry olivine (Hirth and Kohlstedt, 1996) is fit by 9.75 x 10^4 Pa m^{-1} in compression and 4.68 x 10^4 Pa m^{-1} in tension. The mechanical thickness is 60.3 and 63.2 km, respectively.

REFERENCES

Bodine, J.H., M.S. Steckler and A.B. Watts, Observations of flexure and the rheology of the oceanic lithosphere, *J. Geophys. Res.* 86, 3695-3707, 1981

Breivik, A.J., R. Mjelde, P. Grogan, H. Shimamura, Y. Murai and Y. Nishimura, Caledonide development offshore-onshore Svalbard based on ocean bottom seismometer, conventional seismic, and potential field data, *Tectonophysics* 401, 79-117, 2005

Bugge, T., G.Elvebakk, S. Fanavoll, G. Mangerud, M. Smelror, H.M. Weiss, J. Gjelberg, S.E. Kristensen and K. Nilsen, Shallow stratigraphic drilling applied in hydrocarbon exploration of the Nordkapp Basin, Barents Sea, *Mar. Petr. Geol.* 19, 13-37, 2002

Buiter, S.J.H., Surface deformation resulting from subduction and slab detachment, PhD thesis, *Geologica Ultraiectina* 191, 134 pp., 2000

Buiter, S.J.H. and T.H. Torsvik, Horizontal movements in the eastern Barents Sea constrained by numerical models and plate reconstructions, *Geophys. J. Int.*, doi: 10.1111/j.1365-246X.2007.03595.x, 2007

Buiter, S.J.H., M.J.R. Wortel and R. Govers, The role of subduction in the evolution of the Apennines foreland basin, *Tectonophysics* 296, 249-268, 1998

Bungum, H., O. Ritzmann, N., Maercklin, J.-I. Faleide, W.D. Mooney and S.T. Detweiler, Three-dimensional model for the crust and upper mantle in the Barents Sea Region, *EOS Trans. Am. Geophys. Un.* 86, 160-161, 2005

Burov, E.B. and M. Diament, The effective elastic thickness (T_e) of continental lithosphere: What does it really mean?, *J. Geophys. Res.* 100, 3905-3927, 1995

Byerlee, J., Friction of rocks, *Pure appl. Geophys*. 116, 615-626, 1978

Chapman, D.S., Thermal gradients in the continental crust, *Geol. Soc. Spec. Publ.* 24, 63-70, 1986

Chopra, P.N. and M.S. Paterson, The experimental deformation of dunite, *Tectonophysics* 78, 453-473, 1981

Chopra, P.N. and M.S. Paterson, The role of water in the deformation of dunite, *J. Geophys. Res.* 88, 7861-7876, 1984

Cocks, L.R.M. and T.H. Torsvik, Baltica from the late Precambrian to mid-Palaeozoic times: The gain and loss of a terrane's identity, *Earth-Science Reviews* 72, 39-66, 2005

Ebbing, J., C. Braitenberg and S. Wienecke, Insights into the lithospheric structure and the tectonic setting of the Barents Sea region by isostatic considerations, *Geophys. J. Int.*, doi: 10.1111/j.1365-246X.2007.03602.x, 2007

Faleide, J.I., E. Vågnes and S.T Gudlaugsson, Late Mesozoic-Cenozoic evolution of the south-western Barents Sea in a regional rift-shear tectonic setting, *Mar. Petr. Geol.* 10, 186-214, 1993

Goetze, C., Mechanisms of creep in olivine, in: Creep of engineering materials and of Earth, *Phil, Trans. Royal Soc., London*, A, 288 (eds. A. Kelly, A.H. Cook and G.W. Greenwood), 99-119, 1978

Goetze, C. and B. Evans, Stress and temperature in the bending lithosphere as constrained by experimental rock mechanics, *Geophys. J. R. astr. Soc.* 59, 463-478, 1979

Hansen, F.D. and N.L Carter, Creep of selected crustal rocks at 1000 MPa, *Eos Trans. AGU*, 63,437, 1982

Hirth, G. and D.L. Kohlstedt, Water in the oceanic upper mantle; implications for rheology, melt extraction and the evolution of the lithosphere, *Earth planet. Sci. Lett.* 144, 93-108, 1996

Ivanova, N.M., T.S. Sakoulina and Yu.V. Roslov, Deep seismic investigation across the Barents-kara region and Novozemelskiy Fold Belt (Arctic Shelf), *Tectonophysics* 420, 123-140, 2006

Jaeger, J.C. and N.G.W. Cook, Fundamentals of rock mechanics, *John Wiley and Sons*, New York, 585 pp., 1979

Johansen, S.E., B.K. Ostisty, Ø. Birkeland, Y.F. Fedorovsky, V.N. Martirosjan, O. Bruun Christensen, S.I. Cheredeev, E.A. Ignatenko and L.S. margulis, Hydrocarbon potential in the Barents Sea region: play distribution and potential, in: Arctic Geology and Petroleum Potential, *NPF Spec. Publ.* 2 (eds. T.O. Vorren, E. Bergsager, Ø.A. Dahl-Stamnes, E. Holter, B. Johansen, E.Lie and T.B Lund), 273-320, 1993

Mackwell, S., M.E. Zimmerman and D.L. Kohlstedt, High-temperature deformation of dry diabase with application to tectonics on Venus, *J. Geophys. Res.* 103 (1), 975-984, 1998

McAdoo, D.C., J.G. Caldwell and D.L. Turcotte, On the elastic-perfectly plastic bending of the lithosphere under generalized loading with application to the Kuril Trench, *Geophys. J. R. astr. Soc.* 54, 11-26, 1978

McNutt, M.K., M. Diament and M.G. Kogan, Variations of elastic plate thickness at continental thrust belts, *J. Geophys. Res.* 93, 8825-8838, 1988

O'Leary, N., N. White, S. Tull, V. Bashilov, V. Kuprin, L. Natapov and D. MacDonald, Evolution of the Timan-Pechora and South Barents Sea basins, *Geol. Mag*. 151, 141-160, 2004

Otto, S.C. and R.J. Bailey, Tectonic evolution of the northern Ural Orogen, *J. Geol. Soc. London* 152, 903-906, 1995

Ranalli, G., Rheology of the Earth, *Allen and Unwin Inc*., Winchester USA, 366 pp., 1987

Ritzmann, O. and J.I. Faleide, Caledonian basement of the western Barents Sea, *Tectonics*, 26, doi:10.1029/2006TC002059, 2007

Ritzmann, O., N. Maercklin, J.I. Faleide, H. Bungum, W.D. Mooney and S.T. Detweiler, A three-dimensional geophysical model of the crust in the Barents Sea region: Model construction and basement characterisation, *Geophys. J. Int.*, 170, 417-435, 2007

Rutter, E.H. and K.H. Brodie, The role of tectonic grain size reduction in the rheological stratification of the lithosphere, *Geol. Rundschau* 77, 295-308, 1988

Rybacki, E. and G. Dresen, Dislocation and diffusion creep of synthetic anorthite aggregates, *J. Geophys. Res.* 105, 26,017-26,036, 2000

Shelton, G. and J. Tullis, Experimental flow laws for crustal rocks, *EOS Trans. AGU* 62 (17), 396, 1981

Turcotte, D.L. and G. Schubert, Geodynamics, *Cambridge University Press*, 456 pp., 2002

Watts, A.B., An analysis of isostasy in the world's oceans: 1. Hawaiian-Emporer Seamount Chain, *J. Geophys. Res.* 83, 5989-6004, 1978

Watts, A.B., Isostasy and Flexure of the Lithosphere, *Cambridge University Press*, 458 pp., 2001

Watts, A.B. and E.B. Burov, Lithospheric strength and its relationship to the elastic and seismogenic layer thickness, *Earth Planet. Sci. Lett.* 213, 113-131, 2003

Wienecke, S., J. Ebbing and L. Gernigon, 3D density modelling, isostasy and elastic thickness calculation of the Barents Sea, *NGU report*, 2007.022, 2007

Wilks, K.R. and N.L. Carter, Rheology of some continental lower crustal rocks, *Tectonophysics*, 182, 57-77, 1990

Norges geologiske undersøkelse
Postboks 6315, Sluppen
7491 Trondheim, Norge

Besøksadresse
Leiv Eirikssons vei 39, 7040 Trondheim

Telefon 73 90 40 00
Telefax 73 92 16 20
E-post ngu@ngu.no
Nettside www.ngu.no

Geological Survey of Norway
PO Box 6315, Sluppen
7491 Trondheim, Norway

Visitor address
Leiv Eirikssons vei 39, 7040 Trondheim

Tel (+ 47) 73 90 40 00
Fax (+ 47) 73 92 16 20
E-mail ngu@ngu.no
Web www.ngu.no/en-gb/